

Title	Visualization of Chromosome Higher-Order Structure by New Methods
Author(s)	Dwiranti, Astari
Citation	大阪大学, 2014, 博士論文
Version Type	VoR
URL	<a href="https://doi.org/10.18910/50539">https://doi.org/10.18910/50539</a>
rights	
Note	

***Osaka University Knowledge Archive : OUKA***

<https://ir.library.osaka-u.ac.jp/>

Osaka University

**Doctoral Dissertation**

**Visualization of Chromosome Higher-Order Structure**

**by New Methods**

(新手法による染色体高次構造の可視化)

**Astari Dwiranti**

June 2014

Laboratory of Dynamic Cell Biology

Department of Biotechnology

Graduate School of Engineering

OSAKA UNIVERSITY

# Contents

List of abbreviations	i
<b>Chapter 1</b>	
General introduction .....	1
1.1 Chromosome higher-order structure .....	3
1.2 Scanning electron microscopy (SEM) .....	4
1.3 Helium ion microscopy (HIM) .....	6
1.4 Ionic liquid (IL) .....	6
1.5 Focused ion beam/SEM (FIB/SEM) .....	8
1.6 Objective and overview of the study .....	8
<b>Chapter 2</b>	
The effect of divalent cations on chromosome higher-order structure .....	12
2.1 Introduction .....	13
2.2 Materials and Methods	
2.2.1 Sample preparation .....	13
2.2.2 Sample preparation for SEM .....	14
2.2.3 SEM observation .....	15
2.2.4 STEM observation .....	15
2.3 Results	
2.3.1 The effect of $\text{Ca}^{2+}$ on chromosome structure .....	16
2.3.2 The effect of $\text{Mg}^{2+}$ on chromosome structure .....	18
2.3.3 The effect of $\text{Ca}^{2+}$ and $\text{Mg}^{2+}$ on chromosome structure .....	20
2.3.4 The effect of $\text{Mg}^{2+}$ on chromosome observed by STEM tomography.....	22
2.4 Discussion .....	22
2.5 Summary .....	24
<b>Chapter 3</b>	
Uncoated chromosome visualization by helium ion microscopy (HIM) .....	25
3.1 Introduction .....	26

3.2 Materials and Methods	
3.2.1 Sample preparation .....	26
3.2.2 Sample preparation for HIM .....	27
3.2.3 HIM observation .....	27
3.2.4 SEM observation .....	27
3.3 Results	
3.3.1 The effect of OsO <sub>4</sub> coating on chromosome structure observed by SEM .....	28
3.3.2 Uncoated chromosome visualization by HIM .....	29
3.3.3 The effect of OsO <sub>4</sub> coating on chromosome structure visualized by HIM .....	29
3.3.4 The effect of Mg <sup>2+</sup> on chromosome structure visualized by HIM .....	31
3.3.5 The effect of Mg <sup>2+</sup> on chromosome structure visualized by SEM and HIM .....	32
3.5 Discussion .....	33
3.6 Summary .....	35
<b>Chapter 4</b>	
Chromosome observation by scanning electron microscopy using ionic liquid .....	36
4.1 Introduction .....	37
4.2 Materials and Methods	
4.2.1 Sample preparation .....	38
4.2.2 Ionic liquid pretreatment .....	39
4.2.3 Ionic liquid treatment .....	39
4.2.4 SEM observation .....	39
4.2.5 HIM observation .....	39
4.3 Results	
4.3.1 Preliminary experiment .....	39
4.3.2 Chromosome observation after IL treatment .....	41
4.3.3 Chromosomes stained with Pt-blue and prepared with IL .....	44
4.3.4 The effect of Mg <sup>2+</sup> on IL-treated chromosome structure observed by SEM.....	46
4.3.5 Higher resolution chromosome images by combining IL method and HIM.....	47
4.4 Discussion .....	49
4.5 Summary .....	51

## **Chapter 5**

Chromosome interior investigation by FIB/SEM with ionic liquid .....	52
5.1 Introduction .....	53
5.2 Materials and Methods	
5.2.1 Barley chromosome preparation .....	54
5.2.2 PA chromosome pretreatment .....	55
5.2.3 Ionic liquid treatment and critical point drying .....	55
5.2.4 Sectioning and observation by FIB/SEM.....	56
5.2.5 Chromosome 3D visualization by STEM tomography.....	57
5.3 Results	
5.3.1 Chromosome prepared by CPD .....	58
5.3.2 Chromosome prepared with ionic liquid .....	62
5.3.3 Nucleosome-like visualization within chromosome observed by FIB/SEM ...	64
5.3.4 Chromosome visualization by STEM tomography with IL method .....	67
5.4 Discussion .....	68
5.5 Summary .....	69
<b>Chapter 6</b>	
General conclusion .....	71
References .....	76
List of publications .....	83
Acknowledgements .....	84

## List of abbreviations

AM	Acetoxymethyl ester
BAPTA	1,2-bis (2-aminophenoxy) ethane-N,N,N',N'-tetraacetic acid
BMI-BF <sub>4</sub>	1-butyl-3-methylimidazolium tetrafluoroborate
BSE	Backscattered electron
CPD	Critical point drying
EM	Electron microscopy
EMI-BF <sub>4</sub>	1-ethyl-3-methylimidazolium tetrafluoroborate
EMI-Lactate	1-ethyl-3-methylimidazolium lactate
EtOH	Ethanol
FIB	Focused ion beam
FM	Fluorescence microscopy
HIM	Helium ion microscopy
IL	Ionic liquid
OsO <sub>4</sub>	Osmium tetroxide
PA	Polyamine
PBS	Phosphate buffered saline
Pt-blue	Platinum blue
SE	Secondary electron
SEM	Scanning electron microscopy
STEM	Scanning transmission electron microscopy

## **Chapter 1**

### **General introduction**

The understanding of chromosome structure is the basis for determining its function leading to the proper segregation during cell division. Until now, the enigma of how the metaphase chromosome constructed remains unsolved. The continuous and comprehensive study of chromosome higher-order structure and at the same time the development and introduction of new technologies are necessary to answer this mystery. One of the information known about chromosome structure has been that divalent cations especially  $\text{Ca}^{2+}$  and  $\text{Mg}^{2+}$  are required for the organization of chromosomes. However the detailed information about the role of these cations on chromosome organization is still limited.

For chromosome study, electron microscopy including scanning electron microscopy (SEM) has a great advantage because of its high magnification and resolution. SEM uses the signals arising from the interaction of the electrons with the sample to obtain information both about structure and materials composition. However, the utilization of SEM to visualize chromosome higher-order structure is limited because of the time-consuming and multiple sample preparation steps required for biological sample observation. Besides the requirement of drying and dehydration which could distort the biological structure and cause collaption due to the forces of surface tension, the necessity to coat biological sample by metal would also conceal the real structure of the samples. The development of the new methods enabling observation of biological samples without dehydration, drying, and metal coating would be very effective for the biological field including chromosome research.

Helium ion microscopy (HIM) has been developed that resembles SEM in mechanisms but using helium ion beam instead of electron. HIM has many advantages over SEM, such as sub-nanometer resolution, efficient charge control, small beam damage, high depth of field, and nanomachining capability. By using HIM, biological



samples are not required to be coated.

Furthermore, the development of a new method that enables biological samples to be observed not only without metal coating, but also without dehydration and drying, would be a powerful aid to investigating biological samples by SEM. The utilization of ionic liquid (IL) has opened the new perspective in understanding biological phenomena. It allows SEM observation without dehydration, drying, and metal coating because of its high conductivity and negligible volatility. Without dehydration and drying, biological samples treated with IL would maintain their structure in the condition closer to their native one.

For the interior investigation, Focused ion beam/SEM (FIB/SEM) is now receiving increased interest for biological inner structure investigations by performing the slice and view of the samples at nano-order level. FIB/SEM investigation of chromosome structure in conjunction with IL method would be effective for chromosome interior study in the rapid and close to the native way.

### **1.1 Chromosome higher-order structure**

DNA is packaged as chromatin in the interphase nucleus. During mitosis, chromatin fibers are highly condensed to form metaphase chromosomes, which ensure equal segregation of replicated chromosomal DNA into the daughter cells. Chromosomal higher-order structure has biological implications not only for its obvious role in packing long DNA molecules and chromatin fibers into chromosomes, with limited volume before cell division. It also has biological implications for the transportation of DNA fibers to two new daughter cells without damage and the equal distribution of essential proteins to the daughter cells.

The structural details of chromosomes have been of interest for many years and

excellent results have been reported for chromatin structural studies. The fundamental repeating unit of chromatin is the nucleosome that comprises 146 base pairs of DNA wrapped in 1.7 superhelical turns around an octamer of histone proteins and the nucleosomal array, a ‘beads-on-a-string’ fiber with a diameter of 11 nm, represents the first level of chromatin organization has been studied by Luger *et al.* (1997). Early EM studies of native chromatin fibers have led to the proposal of two models for the 30-nm fiber: the one-start helix/solenoid model (Widom and Klug, 1985) and zigzag model (Woodcock and Ghosh, 2010).

Various models of chromosome higher-order structure have been proposed, however the attempts to elucidate chromosome higher-order structure have remained elusive (Fukui and Uchiyama, 2007; Fukui, 2009; Bian & Belmont, 2012). There is long-standing evidence that the integrity of condensed chromatin in the nucleus, as well as in metaphase chromosomes, depends on the binding of cations (Engelhardt, 2004). At high ionic concentrations, chromosomes become granulated and the most frequently observed granules have a diameter of about 35 nm (Caravaca *et al.*, 2005), although the existence of 30 nm chromatin fibers in native chromosomes is still controversial (Eltsov *et al.*, 2008; Grigoryev & Woodcock, 2012; Nishino *et al.*, 2012).

## **1.2 Scanning electron microscopy (SEM)**

Current research in the life sciences requires ultra-high resolution microscopy methods to provide detailed investigation of nanoscale structures, such as chromatin fibers at high resolution. SEM has long been used to gain new insights into the organization of biological structure, macromolecular complexes and interactions of cellular components as well as isolated cell organelles and chromosome because it has higher resolution and magnification than optical microscopy (Schatten, 2011). SEM can

image sample surfaces by scanning them with an electron beam.

For biological samples, a conventional preparation method of SEM samples consists of multiple procedures including fixation, dehydration, drying, conductive staining with metal and mounting on a specimen stub. The column of electron microscopy is in a high vacuum. Vacuum condition is one of the essential requirements for ultra precise analyses at the molecular and atomic levels because all atoms and molecules other than target species are excluded under the observation. Ordinary solvents like water and alcohols evaporate easily with high vapor pressures in the column (Yoshida *et al.*, 2007). Dehydration is being used routinely to prepare samples for viewing in a vacuum environment. However, dehydration can distort the structure of the sample because the shape of a macromolecule or membrane is produced and maintained by its interactions with water molecules which can be destroyed by removing water molecules during the dehydration process. As much as 30-60% shrinkage has been reported after preparing soft tissue for SEM (Boyde and Maconnachie, 1979). Drying may also distort ultrastructure and induce artifacts which have been shown by Ris (1985).

If a sample has no or low conductivity, the electron beam irradiation accumulates charges on its surface and results in serious damage to the SEM images. This charging up phenomenon is prevented by the conductive treatments including metal coating. Coating is important for biological structure to give electric conductivity to the sample by vacuum deposition of a metal. Otherwise, the insulating sample must be charged by irradiation of the electron beam, giving a low-quality image accompanied with lots of noise and distortion (Kuwabata *et al.*, 2010). Consequently the whole procedure for SEM sample preparation requires sophisticated methods and long preparatory time. In addition, metal coating can ultimately lead to misinterpretation of the data obtained. Thus, the development of new methods may solve the problems.

Scanning transmission electron microscopy (STEM) has similarities to the SEM. a highly focused beam of electrons is scanned over the specimen and electrons that pass through the sample are collected to fabricate transmission images. This system has the ability to collect secondary electrons in the same way as a SEM. Furthermore, STEM can be used to generate projection images and reconstruct three-dimensional (3D) images. The 3D structural information in electron tomography is reconstructed digitally from a tilt-series of 2D projections, where images are acquired by tilting the sample to cover a total tilt-range of about  $\pm 60^\circ$ . The tilt-series is then processed off-line using back-projection techniques to reconstruct the original 3D structure (Frank, 1992).

### **1.3 Helium ion microscopy (HIM)**

HIM resembles SEM in its general architecture and mechanism, but uses positively charged helium ions instead of negatively charged electrons to image the sample in the chamber. It has the desirable properties of high contrast, efficient charge control, low beam damage, high depth of field, nanomachining capability, and is ultimately expected to produce images with 0.25 nm resolution (Ward *et al.*, 2006; Bell, 2009). With an electron flood gun set in the sample chamber, metal coating is not required even for nonconductive samples, because the positive surface charging can be neutralized by the electron generated from the flood gun during scanning. Therefore, HIM is considered to be a promising tool for imaging and analyzing the surfaces of biological samples in detail.

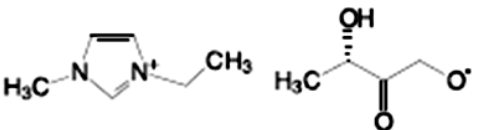
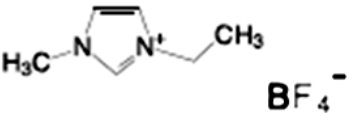
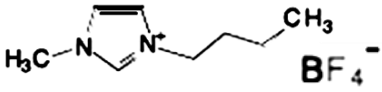
### **1.4 Ionic liquid (IL)**

IL is a synthetic molecular liquid that contains both a positive ion (cation) and a negative ion (anion) that possesses attractive features such as a negligible vapor pressure ( $\leq 5 \times 10^{-9}$  Torr), high ionic conductivity ( $\leq 120 \text{ mS cm}^{-1}$ ), wide liquidus temperature range (173-450 K), non-combustibility, wide electrochemical windows ( $\leq 5.8 \text{ V}$ ), good

dissolving powers, and easily tunable physicochemical properties (Kuwabata *et al.*, 2010, Earle and Seddon, 2000; Hagiwara and Ito, 2000; Welton, 1999). While many solvents will freeze or boil across a large temperature range, IL maintains its volume and fluidity (Forsyth *et al.*, 2004).

The number of combinations of anions and cations, which can be used to produce IL, is in the range of one million. Typical cations includes imidazolium, pyridinium, ammonium, phosphonium, and sulfonium ions, whereas typical anions includes the halogen anions, nitrate, perchlorate, tetrafluoroborate, hexafluorophosphate, bis(trifluoromethanesulfonyl) amide, and toluene-4-sulfonate. Reaction of an imidazolium halide with a tetrafluoroborate in an appropriate solvent will yield a solution of the imidazolium tetrafluoroborate and a metal halide precipitate. 1-ethyl-3-methylimidazolium tetrafluoroborate (EMI- $\text{BF}_4$ ) has been reported in 1992 by Wilkes and Zaworotko as one of the first air- and water-stable IL. It is transparent liquid like water but its viscosity (38 mPa.s at 25°C) is a slightly higher than that of water (1.0 mPa.s at 25°C).

Table 1. Molecular structure of IL.

Name	Molecular structure
1-Ethyl-3-methylimidazolium (l)-lactate (EMI-lactate)	
1-Ethyl-3-methylimidazolium tetrafluoroborate (EMI- $\text{BF}_4$ )	
1-Butyl-3-methylimidazolium tetrafluoroborate (BMI- $\text{BF}_4$ )	

The anions of IL are usually classified by the point whether the anion tends to be hydrophilic or hydrophobic. This will greatly affect the tendency of the ionic liquid to form bonds to the substrate that it is deposited on (Palacio and Bhushan, 2010). 1-ethyl-3-methylimidazolium tetrafluoroborate (EMI-BF<sub>4</sub>) and 1-butyl-3-methylimidazolium tetrafluoroborate (BMI-BF<sub>4</sub>) are imidazolium compounds with high hydrophilicities.

By considering its properties, the finding that IL behaves like an electronic conducting material for EM observation (Kuwabata *et al.*, 2006; Okazaki *et al.*, 2008) led to an idea of observing biological samples by IL. Observation of an EMI-BF<sub>4</sub> drop gave a dark image that is completely different from the SEM image of a silicon oil drop exhibiting charge-up effect. In case of IL, it was confirmed that electrons injected into IL were solvated by condensed ions, allowing electrons to move out of IL (Ishigaki *et al.*, 2011).

### **1.5 Focused ion beam/SEM (FIB/SEM)**

FIB/SEM system is equipped with a focused Ga<sup>+</sup> beam column, used to sequentially mill away the sample surface, as well as an electron beam column to image the milled surfaces directly, generating a large image sequence that can be combined into a 3D image (Bushby *et al.*, 2011). An important aspect of the FIB is the high efficiency with which atoms of the sample can be removed (sputtered). This gives the possibility to selectively mill material to make cross-sections. The application of FIB/SEM for biological samples has just been started (Drobne *et al.*, 2007; Friedmann *et al.*, 2011).

### **1.6 Objective and overview of the study**

Divalent cations have long been studied to have a role for the chromosome organization. However, the overall higher-order structure of chromosomes remains an

enigma in spite of the efforts of numerous researchers, and dozens of different models have been presented. Furthermore, the development and introduction of new technologies particularly for the visualization of chromosome structure by maintaining their conditions as close to the native as possible would be advantageous to gain information of chromosome surface structure and interior. Thus, the objective of this study is to investigate the higher-order structure of chromosome and to develop the new methods which enable chromosome visualization without dehydration, drying, and metal coating, to overcome the drawbacks of conventional sample preparation methods which are laborious, time-consuming, and can distort the chromosome structure.

Chapter 2 will focus on the effect of  $\text{Ca}^{2+}$  and  $\text{Mg}^{2+}$  on chromosome structure. Previous studies showed that the chromosome structure is affected by cations.  $\text{Ca}^{2+}$  and  $\text{Mg}^{2+}$  are abundant divalent cations in the cells and contributed to the maintenance of chromosome structure. However, the detailed information about their role on chromosome organization especially regarding the presence of 30 nm has not been confirmed yet. In this study, the effect of  $\text{Ca}^{2+}$  and  $\text{Mg}^{2+}$  concentrations on chromosome structure were investigated by using optical microscopy and SEM, particularly the reversibility of 11-30 nm chromatin particles. Furthermore, the advantages of STEM tomography in providing 3D information of chromosome images by tilting the sample stage were also assessed to gain the more detailed results of chromosome structure in different concentration of  $\text{Mg}^{2+}$ .

Chapter 3 will deal with the visualization of chromosome by HIM. This system enables biological sample observation even without metal coating. Its high resolution and wide depth of field also provides promising results compared with SEM. Thus in this study, this newly developed system was used for the study of chromosome structure without metal coating. The effect of  $\text{OsO}_4$  coating is first described in Chapter 3, followed

by the different structure of chromosome with and without coating. The structure of uncoated chromosome in different concentration of  $\text{Mg}^{2+}$  was also revealed.

Chapter 4 described the development of IL method for SEM. Not only had the usage of HIM, in this study, the advantages of IL method in enabling SEM observation without dehydration, drying, and metal coating were also evaluated for the first time to visualize chromosomes. The employment of IL method for SEM observation would be suitable to maintain the samples in the condition closer to their native one and to avoid the bias of the artifacts induced during sample preparation. The optimum conditions for chromosome observation with the IL method have further been determined. In addition, the IL method was explored more by combining it with the HIM to obtain the higher resolution chromosome images.

Chapter 5 presented the chromosome interior taken by FIB/SEM. In order to gain the detailed information of chromosome higher-order structure, FIB/SEM was used for the structural investigation of chromosome interior by slicing the chromosome and direct viewing its structure at nano-order level. Chromosome structure prepared with conventional method including drying by critical point drying (CPD) and those prepared with IL method were evaluated. The first observation of chromosome interior prepared with IL gave a new perspective of the structure within chromosome. For the whole chromosome 3D observation without sectioning, in this chapter, the introduction of IL method to STEM tomography was also described. The combination of IL method with FIB/SEM and STEM tomography were demonstrated to be beneficial for chromosome interior and 3D imaging in rapid and less laborious manner.

Finally in Chapter 6, the major results of this study were summarized and the conclusion was given based on the whole data obtained. The general idea of this research is presented in Figure 1.



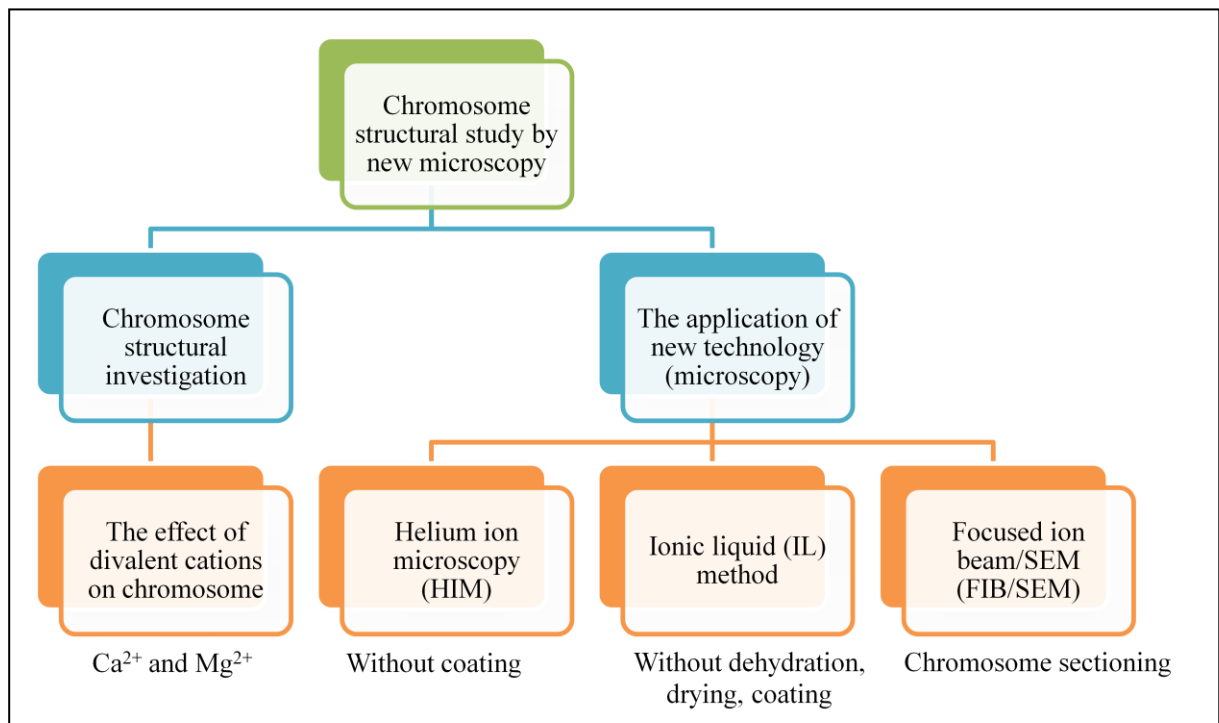


Figure 1. The research flow of chromosome study by new visualization methods.

## **Chapter 2**

### **The effect of divalent cations on chromosome higher-order structure**

## 2.1 Introduction

To investigate the effect of  $\text{Ca}^{2+}$ , the  $\text{Ca}^{2+}$  chelator 1,2-bis (2-aminophenoxy) ethane-N,N,N',N'-tetraacetic acid (BAPTA) or a cell-permeant chelator BAPTA acetoxymethyl ester (BAPTA AM) was applied. Chromosome structure with and without BAPTA (AM) was compared.

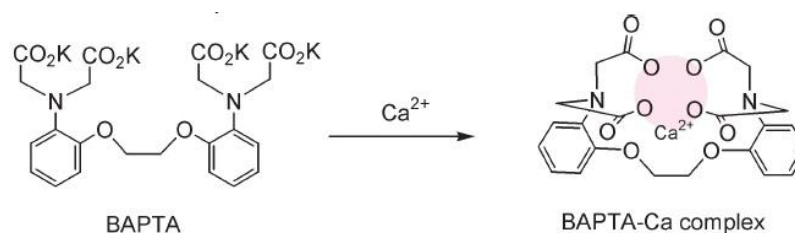


Figure 2. BAPTA as the  $\text{Ca}^{2+}$  chelator.

Different concentrations of  $\text{Mg}^{2+}$  (0 and 5 mM) were also applied to study the effect of  $\text{Mg}^{2+}$  on chromosome structure. The reversibility of the chromatin diameter upon the re-addition of  $\text{Ca}^{2+}$  and  $\text{Mg}^{2+}$  was evaluated. Finally, both  $\text{Ca}^{2+}$  and  $\text{Mg}^{2+}$  were depleted by using Ethylenediaminetetraacetic acid (EDTA) which has affinity to chelate both ions. Chromosomes were visualized by optical microscopy and SEM.

## 2.2 Materials and Methods

### 2.2.1 Sample preparation

In this study, chromosomes from HeLa S3 cells originated from human cervical adenocarcinoma were investigated. Chromosomes were either spread on coverslips using centrifugation (spread chromosomes) or isolated and suspended by polyamine method (PA isolated chromosomes, Uchiyama *et al.*, 2004, 2005; Hayashihara *et al.*, 2008). To investigate the effect of  $\text{Ca}^{2+}$  concentration changes on chromosome structure, BAPTA (Dojindo) was applied to chelate  $\text{Ca}^{2+}$  directly from isolated chromosomes, and BAPTA AM (Dojindo) was used to deplete  $\text{Ca}^{2+}$  by adding it into the cell culture where the spread

chromosomes were prepared from.

Cells were synchronized by adding 0.1% v/v colcemid (Sigma Aldrich) for 3 hours. To evaluate the effect of  $\text{Ca}^{2+}$  on spread chromosome, 20  $\mu\text{M}$  BAPTA AM was added into HeLa S3 cell culture (0.1% v/v) after 1.5 h colcemid treatment to chelate  $\text{Ca}^{2+}$  (PBS for control; 137 mM NaCl, 2.7 mM KCl, 10 mM  $\text{Na}_2\text{HPO}_4$ , 1.8 mM  $\text{KH}_2\text{PO}_4$ , pH = 7.4). Cells were centrifuged, washed, and then subjected to hypotonic treatment (75 mM KCl 15 min). After that, spread chromosomes were obtained by using centrifugation (Shandon Cytospin 4, Thermo) and treated with 0.5% Triton X-100 (Sigma Aldrich) in Milli-Q water. Some samples were subjected to 20  $\mu\text{M}$   $\text{Ca}^{2+}$  re-addition to observe the reversibility of chromosome structure. After these  $\text{Ca}^{2+}$  treatments, some samples were stained with 4',6-diamidino-2-phenylindole (DAPI) and observed by optical microscope (Axioplan 2, Zeiss). The rest of the samples were subjected to preparation for SEM.

Besides  $\text{Ca}^{2+}$  treatment, some chromosomes were treated with buffers containing different concentration of  $\text{Mg}^{2+}$ . Chromosomes were placed on a coverslips, incubated on ice for 10 min, and then subjected to two different buffers for 30 min, XBE (10 mM HEPES, pH 7.7, 100 mM KCl, and 5 mM EGTA) and XBE5 (10 mM HEPES, pH 7.7, 5 mM  $\text{MgCl}_2$ , 100 mM KCl, and 5 mM EGTA). Samples were then either stained with DAPI for optical microscopy (Axioplan 2, Zeiss) observation or subjected to preparation for SEM. Similar preparation was also performed in order to evaluate the effect of both  $\text{Ca}^{2+}$  and  $\text{Mg}^{2+}$  using 1 mM EDTA (Dojindo).

### **2.2.2 Sample preparation for SEM**

Chromosomes on the coverslips were fixed with 2.5% glutaraldehyde diluted in XBE5 or XBE buffer and 0.2% tannic acid/XBE5 or XBE, post-fixed with 2%  $\text{OsO}_4$ /Milli-Q, and then washed by using Milli-Q water three times, 5 min each. They

were subsequently dehydrated with EtOH 70, 100, 100%, dried by Critical Point Dryer (JCPD-5, JEOL, Tokyo, Japan), coated with OsO<sub>4</sub> coater (HPC-1S; Vacuum Device Inc., Japan) and finally observed by SEM.

### **2.2.3 SEM observation**

Chromosomes were observed by SEM S-5200 (Hitachi, Tokyo, Japan) with the accelerating voltage of 10 kV in secondary electron (SE) mode. In this system, the distance between objective lens and sample stage is fix and close. Thus, instead of adjusting the Z value (working distance), magnification setting was performed by adjusting the currents of the objective lens. SEM data in pixels were analyzed by using ImageJ software (Abramoff et al., 2004). The diameters of chromatin particles (n = 30-50 particles) were measured randomly from each chromosome (3-5 chromosomes per each treatment).

### **2.2.4 STEM observation**

Chromosomes were dropped on TEM grid (75 mesh) for 10 min on ice. Samples were then washed and treated with buffer containing 0 and 5 mM Mg<sup>2+</sup> for 30 min. After that, they were subjected to 2.5% glutaraldehyde and 0.2% tannic acid fixation diluted in either XBE or XBE5 buffer 30 min, OsO<sub>4</sub> post-fixation 15 min, washing three times 5 min each, and followed with the EtOH series dehydration. Drying was performed by using critical point dryer. Finally the samples were coated by carbon coater and observed by STEM tomography (Tecnai G<sup>2</sup>, FEI). Sample stage was tilted every 2° from -60° to +60° and image series were taken at each position.

## 2.3 Results

### 2.3.1 The effect of $\text{Ca}^{2+}$ on chromosome structure

The results of optical microscopy observation showed that chromosomes structure with and without  $\text{Ca}^{2+}$  chelation was different (Fig. 3). Chromosomes were more expanded and dispersed after  $\text{Ca}^{2+}$  depletion compared with the control.

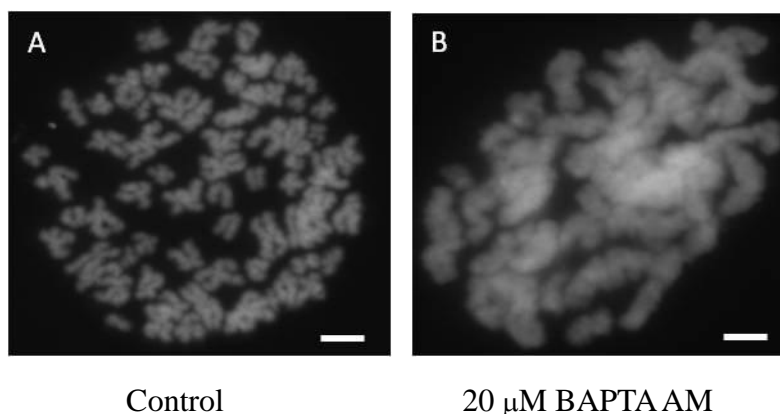


Figure 3. Chromosome structure was changed with the depletion of  $\text{Ca}^{2+}$ . Chromosomes treated with BAPTA AM ( $\text{Ca}^{2+}$  chelator) showed the more dispersed and expanded structure (B) compared with the control (A). Bars: 10  $\mu\text{m}$ .

Consistent with FM results, SEM results also showed that the chromosome structure and the diameter of chromatin fibers were varied with the different treatments. Chromatin particles of the chromosome treated with BAPTA AM were smaller compared with the control. Interestingly, chromosome structure was returned after  $\text{Ca}^{2+}$  re-addition (Fig.4).

To get a quantitative data, the mean diameter of chromatin particles was measured. Yellow bars shown in Fig. 4C' illustrate the diameter measurement of chromatin particles. Measurement was performed by using ImageJ software with the known distance was set according to the data taken by SEM. According to the data, the mean diameter of chromatin fiber was changed from  $34.18 \pm 5.38$  (mean  $\pm$  SD) nm of the control into  $13.83 \pm 2.94$  nm after  $\text{Ca}^{2+}$  depletion and returned to  $32.32 \pm 4.16$  nm after 20  $\mu\text{M}$   $\text{Ca}^{2+}$  re-addition (Fig.5). These results suggest that the chromosome structure and the diameter of chromatin fiber are most likely to be reversible upon different concentration of  $\text{Ca}^{2+}$ .

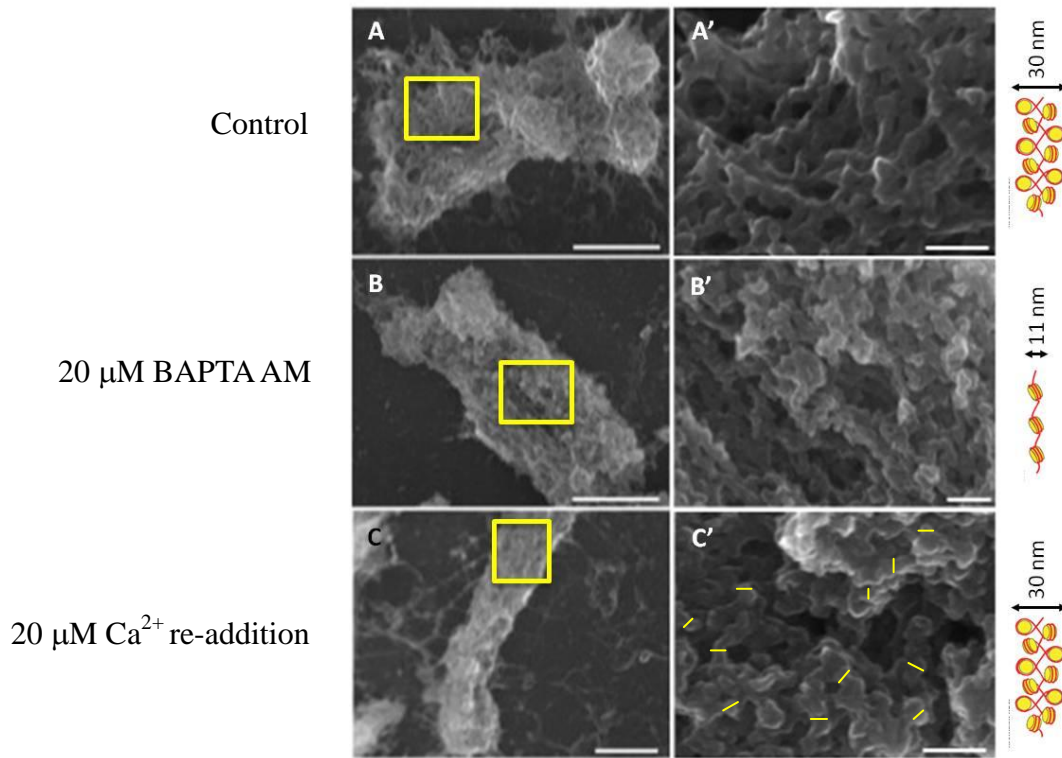


Figure 4. The diameter of chromatin fiber was changed with  $\text{Ca}^{2+}$  depletion and returned after  $\text{Ca}^{2+}$  re-addition. The diameter of chromatin in control (A, A') was larger compared with the chromatin after 20  $\mu\text{M}$  BAPTA AM treatment (B, B'). Similar chromatin diameter with control was achieved after re-addition of 20  $\mu\text{M}$   $\text{Ca}^{2+}$  (C, C'). Bars: 1  $\mu\text{m}$  (A, B, C), 100 nm (A', B', C').

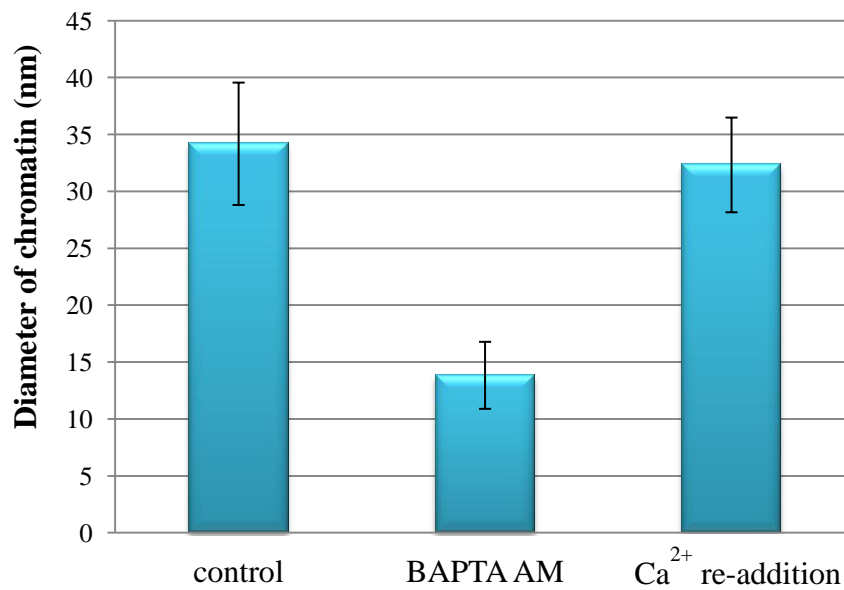


Figure 5. The effect of  $\text{Ca}^{2+}$  on chromatin structure. The mean diameter of chromatin fiber was decreased with  $\text{Ca}^{2+}$  depletion and returned after  $\text{Ca}^{2+}$  re-addition.

### 2.3.2 The effect of $Mg^{2+}$ on chromosome structure

Buffers containing 5 (XBE5) and 0 mM (XBE)  $Mg^{2+}$  were prepared to evaluate the effect of  $Mg^{2+}$  on chromosome structure. The different structure of chromosome in different  $Mg^{2+}$  concentration was observed by FM (Fig.6) and SEM (Fig.7). Chromosomes maintained their compact structure with the presence of 5 mM  $Mg^{2+}$  and turned into the more dispersed structure when they were treated with buffer lack of  $Mg^{2+}$ .

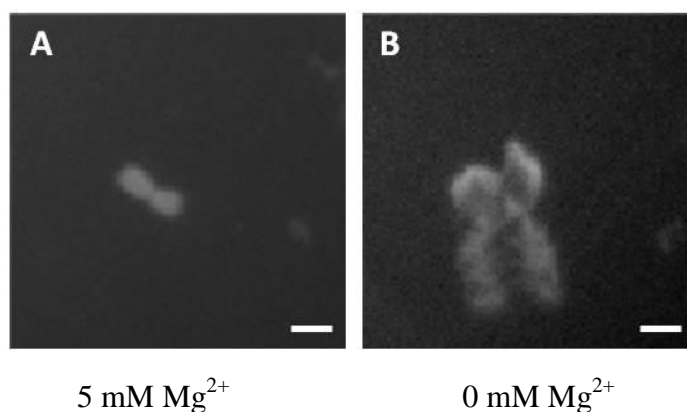


Figure 6. Chromosome structure was varied upon  $Mg^{2+}$  concentration. Chromosome maintained its structure when it was treated with buffer containing 5 mM  $Mg^{2+}$  (A) and dispersed when it was treated with buffer containing 0 mM  $Mg^{2+}$  (B). Bars: 1  $\mu$ m.

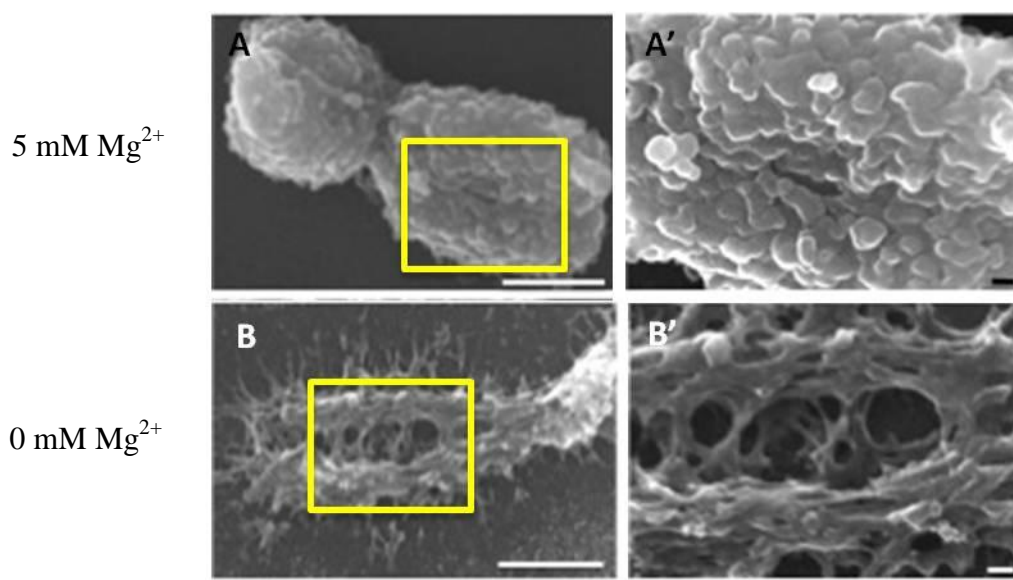


Figure 7. Chromosome structure was different in different concentration of  $Mg^{2+}$ . Chromosome treated with buffer containing 5 mM  $Mg^{2+}$  showed the more compact structure (A, A'), and the structure became distorted when the chromosome was treated with buffer containing no  $Mg^{2+}$  (B, B'). Bars: 1  $\mu$ m (A, B), 100 nm (A', B').



Similar to the effect of  $\text{Ca}^{2+}$ , the changes of chromosome structure upon  $\text{Mg}^{2+}$  concentration underwent reversible manner as well. The chromatin particles were smaller in the chromosome treated with the buffer containing no  $\text{Mg}^{2+}$  compared with those treated with buffer containing 5 mM  $\text{Mg}^{2+}$ . Re-addition of 5 mM  $\text{Mg}^{2+}$  resulted in the returning mean diameter of the chromatin particles observed by SEM (Figs. 8 and 9).

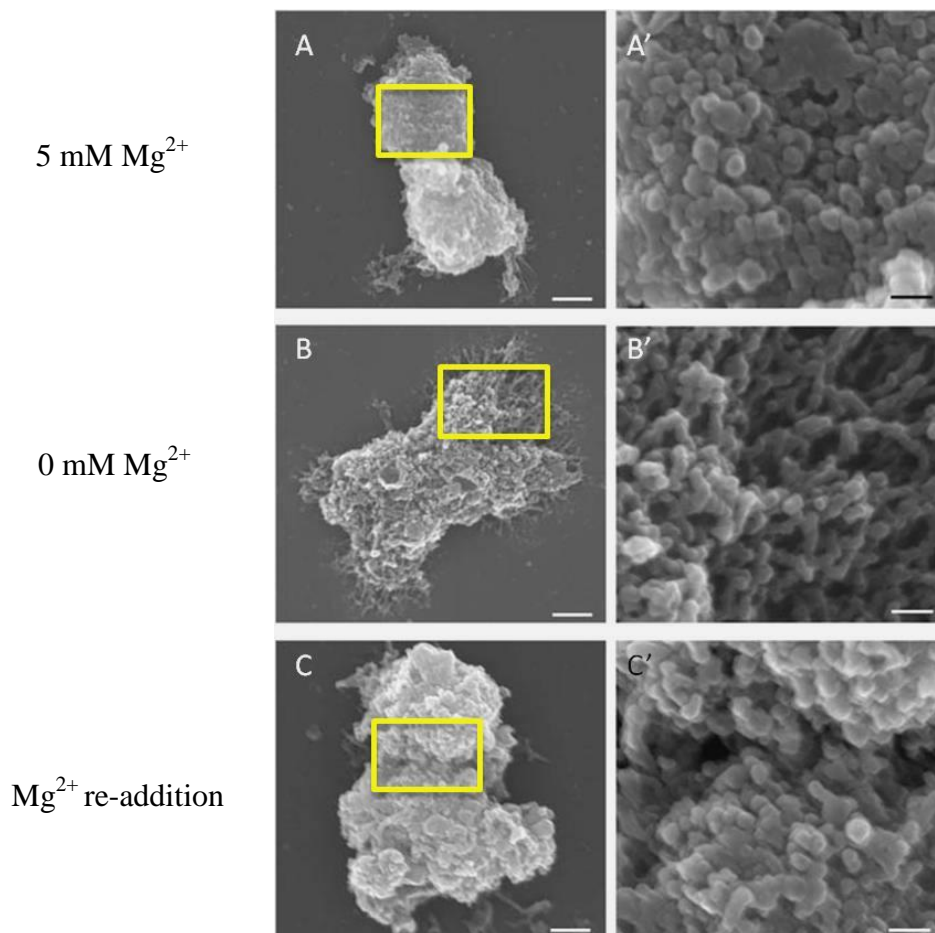


Figure 8. The diameter of chromatin fiber was different upon different  $\text{Mg}^{2+}$  concentration. The diameter of chromatin in 5 mM  $\text{Mg}^{2+}$ -treated chromosome (A, A') was larger compared with the chromatin treated with 0 mM  $\text{Mg}^{2+}$  (B, B'). Similar chromatin diameter with control was achieved after re-addition of 5 mM  $\text{Mg}^{2+}$  (C, C'). Bars: 100 nm (A', B', C').

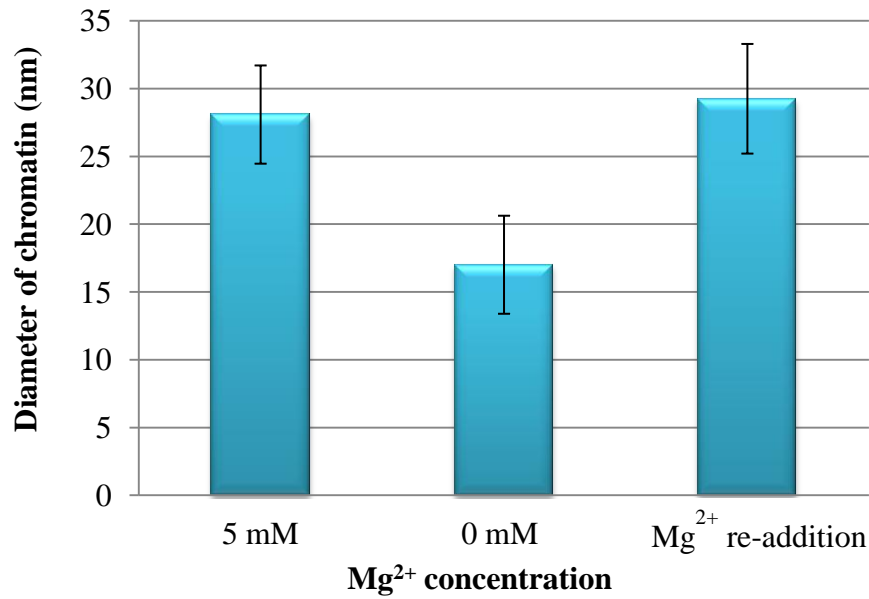


Figure 9. The effect of Mg<sup>2+</sup> on chromatin structure. The mean diameter of chromatin particles was changed from 28.08 ± 3.62 (mean ± SD) in 5 mM Mg<sup>2+</sup> treatment into 17.01 ± 3.61 in 0 mM Mg<sup>2+</sup>, and returned to 29.25 ± 4.04 after Mg<sup>2+</sup> re-addition.

### 2.3.3 The effect of Ca<sup>2+</sup> and Mg<sup>2+</sup> on chromosome structure

The effect of both Ca<sup>2+</sup> and Mg<sup>2+</sup> depletion using EDTA treatment was also investigated. The observation by FM shows that chromosome structure became expanded after this treatment (Fig.10). In addition, the reversibility phenomenon could be visualized on the chromosome after the re-addition of either Mg<sup>2+</sup> or Ca<sup>2+</sup> (Fig.11). The SEM images of chromosomes in different Ca<sup>2+</sup> and Mg<sup>2+</sup> concentration were summarized in Figure 12.

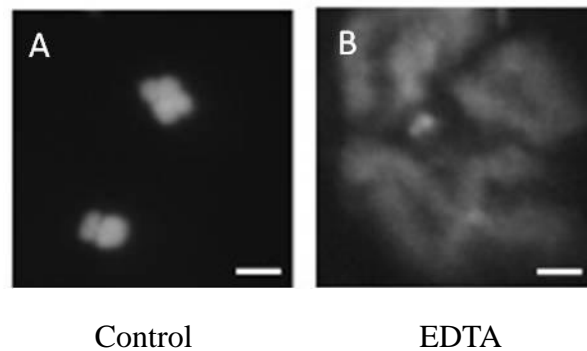


Figure 10. Chromosomes showed a longer and dispersed structure after Ca<sup>2+</sup> and Mg<sup>2+</sup> depletion (B) compared with the control (A). Bars: 1 µm.

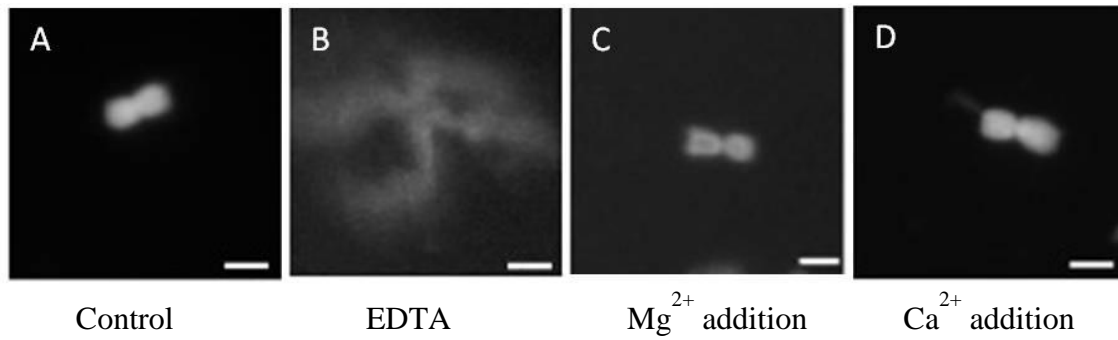


Figure 11. Chromosomes were expanded after  $\text{Ca}^{2+}$  and  $\text{Mg}^{2+}$  depletion by EDTA (B) compared with control (A), and reversible after either  $\text{Ca}^{2+}$  (C) or  $\text{Mg}^{2+}$  (D) addition. Bars: 1  $\mu\text{m}$ .

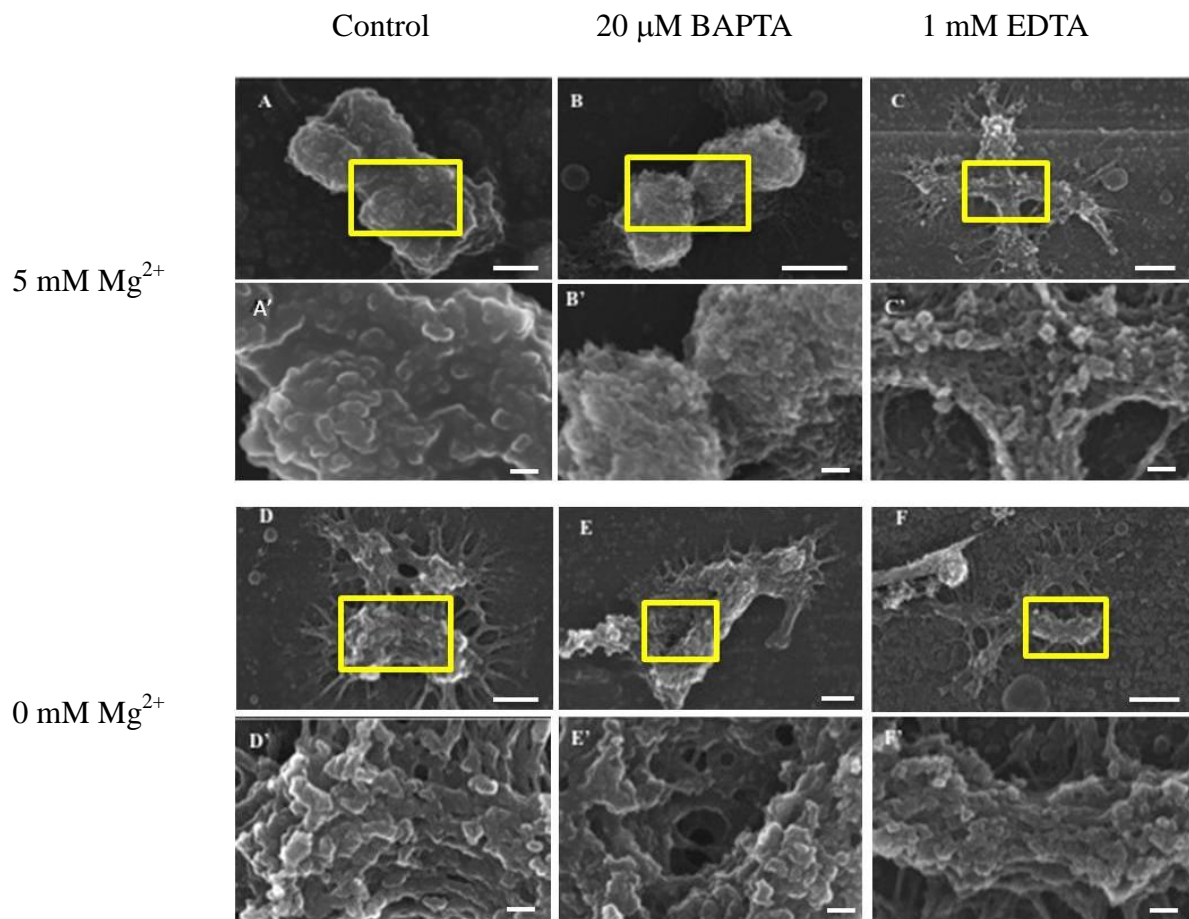


Figure 12. Chromosome structure was varied upon  $\text{Ca}^{2+}$  and  $\text{Mg}^{2+}$  concentration. Chromatin diameters were smaller in  $\text{Ca}^{2+}$ -depleted (B), EDTA- (C) and 0 mM  $\text{Mg}^{2+}$ -treated samples (D, E, F) compared with the control (A). Global structure of chromosome was also distorted in EDTA- and 0 mM  $\text{Mg}^{2+}$ - treated samples. Figures A'-F' showed the high magnification images indicated by the yellow boxes of each chromosome. Bars: 500 nm (A, B, C, D, E, F), 100 nm (A', B', C', D', E', F')

### 2.3.4 The effect of $Mg^{2+}$ on chromosome observed by STEM tomography

Lastly, to gain deeper information regarding chromosome structure in different  $Mg^{2+}$  concentration viewed from different position, STEM tomography observation was conducted. Chromosomes were prepared with buffer containing 5 and 0 mM  $Mg^{2+}$  on TEM grid. Samples were tilted every  $2^\circ$  from  $-60^\circ$  to  $+60^\circ$ . Chromosome images taken at  $0^\circ$  are shown in Figure 13.

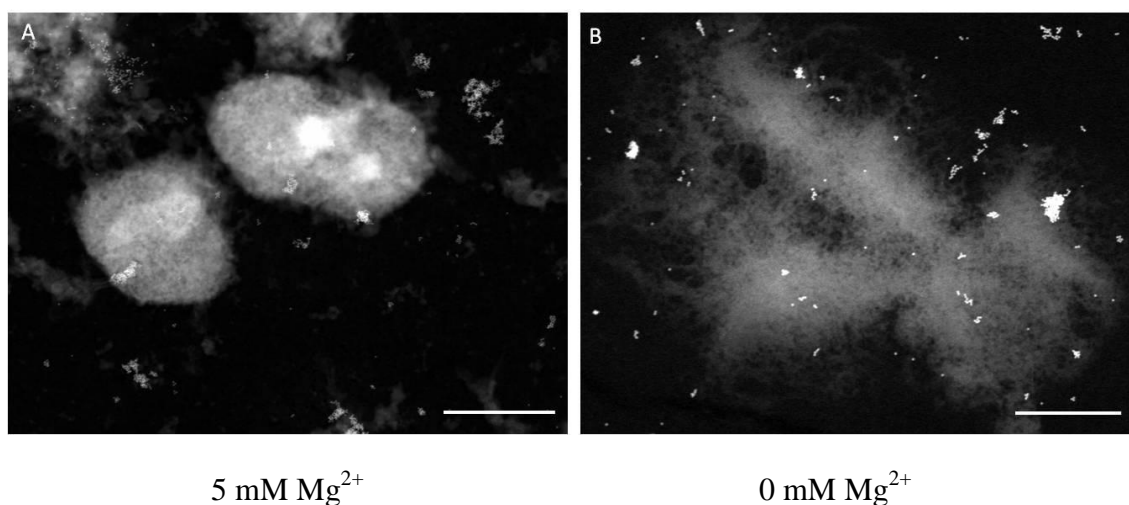


Figure 13. STEM tomography showed the different structure of chromosome in different  $Mg^{2+}$  concentration. Chromosomes were compact when they were treated with 5 mM  $Mg^{2+}$  (A) and became dispersed when it was treated with buffer containing 0 mM  $Mg^{2+}$  (B). Bars: 1  $\mu$ m.

## 2.4 Discussion

In this study, the role of divalent cations ( $Ca^{2+}$  and  $Mg^{2+}$ ) in chromosome higher-order structure, particularly the reversibility of c.a. 11-30 nm chromatin particles is evaluated. The structure of chromosomes in different concentrations of  $Ca^{2+}$  and  $Mg^{2+}$  was observed by FM and SEM.

Based on the data obtained, the chromosome structure and the diameter of chromatin fibers were varied with the different treatments. Chromatin particles of the chromosome treated with BAPTA AM were smaller compared with the control indicating the

importance of  $\text{Ca}^{2+}$ . In addition, chromosome treated with buffer containing 0 mM  $\text{Mg}^{2+}$  showed the more disperse structure compared with 5 mM  $\text{Mg}^{2+}$ -treated one, suggesting that the sufficient concentration of  $\text{Mg}^{2+}$  is necessary to maintain chromosome structure.

Chromosomes treated with 5 mM  $\text{Mg}^{2+}$  showed the more condensed structure and larger chromatin diameter compared with those treated without  $\text{Mg}^{2+}$ . Chromosome structure was also distorted after EDTA treatment, suggesting that EDTA plays a role in chelating  $\text{Mg}^{2+}$  which resulted in the similar structural deformation. Chromosome structure was reversible after the re-addition of either  $\text{Ca}^{2+}$  or  $\text{Mg}^{2+}$ . An adequate concentration of divalent cations is required for the organization and maintenance of chromosome higher-order structure. A high  $\text{Mg}^{2+}$  concentration preserves chromosomes in a condensed state.

The disperse structure of chromatin fiber when it was treated with buffer lack of  $\text{Mg}^{2+}$  was also shown by STEM tomography. This system enables us to visualize a whole chromosome in three dimensions without sectioning which is difficult to be obtained by conventional TEM. The different structure of chromosome in different concentration of  $\text{Mg}^{2+}$  was clearly determined from each tilting angles. Not only the disperse chromatin fibers; the expanded global structure could also clearly be defined by STEM tomography when the chromosome was treated with 0 mM  $\text{Mg}^{2+}$ .

## 2.5 Summary

To summarize, chromosome structure was affected by divalent cations ( $\text{Ca}^{2+}$  and  $\text{Mg}^{2+}$ ). Both  $\text{Mg}^{2+}$  and  $\text{Ca}^{2+}$  are important for the chromosome organization, especially in the organization of c. a. 11 to 30 nm chromatin structures. In addition, the changes of chromosome structure in different concentration of divalent cations undergo the reversibility manner. Furthermore, in this study, the compact structure of chromosome in 5 mM  $\text{Mg}^{2+}$  and the dispersed and expanded structure of chromosome when the  $\text{Mg}^{2+}$  was absent were presented for the first time in three-dimensions by STEM tomography.

## **Chapter 3**

### **Uncoated chromosome visualization by helium ion microscopy (HIM)**

### **3.1 Introduction**

The use of SEM for biological samples observation including chromosome is limited by the multistep preparation which is time-consuming and can induce artifact. For example, the metal coating can form a deposit on the top of the sample, rendering a false surface structure (Pretorius, 2010). The development of a method that enables biological samples to be observed without coating would greatly aid the study of biological structures, such as chromosomes.

HIM, which has recently been developed, may solve the problem because it does not require sample coating due to its charge compensation system. However, HIM has not yet been used for the investigation of detailed chromosome structure. The observation of the surface structure of uncoated chromosomes by HIM was conducted in this study. In order to study the effect of  $\text{Mg}^{2+}$  concentration on chromosome structure by HIM, chromosomes treated with 5 and 0 mM  $\text{Mg}^{2+}$  ions were prepared.

### **3.2 Materials and Methods**

#### **3.2.1 Sample preparation**

Chromosomes were placed on a silicon substrate ( $\text{SiO}_2$  substrates), incubated on ice for 10 min, and then subjected to two different buffers, XBE5 (5 mM  $\text{Mg}^{2+}$ ) and XBE (0 mM  $\text{Mg}^{2+}$ ) for 30 min, followed by fixation with 2.5% glutaraldehyde/XBE5 or 2.5% glutaraldehyde/XBE and 0.2% tannic acid/XBE5 or 0.2% tannic acid/XBE at room temperature for 30 min, and then washed with XBE5 or XBE buffers three times, 5 min each.



### **3.2.2 Sample preparation for HIM**

After fixation, samples were then postfixed with 2% OsO<sub>4</sub>/Milli-Q, and washed by using Milli-Q water. After that, they were subsequently dehydrated with a series of 70, 100, and 100% EtOH, and then dried in a critical point dryer (JCPD-5, JEOL, Tokyo, Japan). Uncoated samples were then directly observed by HIM, while coated samples were prepared by subjecting the samples to OsO<sub>4</sub> coating for 15 sec prior to HIM observation.

### **3.2.3 HIM observation**

A number of chromosomes were observed to obtain an overall view of chromosome general morphology. High magnification images of the chromosome surface were also recorded to visualize chromatin more clearly. The HIM (Orion Plus, Zeiss, Oberkochen, Germany) was operated at an accelerating voltage of 30 kV, a beam current of 0.2 pA, and working distance of 6.4 mm. The HIM images were processed with a median filter (2.0 pixel radius) and normalized by using ImageJ. Chromatin diameter was also measured using ImageJ software.

### **3.2.4 SEM observation**

To investigate the effect of OsO<sub>4</sub> coating on chromatin mean diameter, some chromosomes were subjected to different OsO<sub>4</sub> coating times, ranging from 2.5 to 17.5 s by using an osmium coater (HPC-1S; Vacuum Device Inc., Japan). They were then observed by high-vacuum SEM (S-5200, Hitachi, Tokyo, Japan) in secondary electron mode using an electron voltage of 10 kV. The mean chromatin diameters for various regions (centromere, chromosome arms, and telomere) were calculated from each sample set (n = 150-300).

### 3.3 Results

#### 3.3.1 The effect of OsO<sub>4</sub> coating on chromosome structure observed by SEM

Chromatin diameter dynamics with different OsO<sub>4</sub> coating treatments are shown in Figure 14. Scanning electron micrographs of chromosomes coated with OsO<sub>4</sub> for 2.5 s (Figs. 14A, A'), 10 s (Figs. 14B, B'), and 17.5 s (Figs. 14C, C'), indicate chromatin diameter increases linearly with longer coating times (Fig. 15).

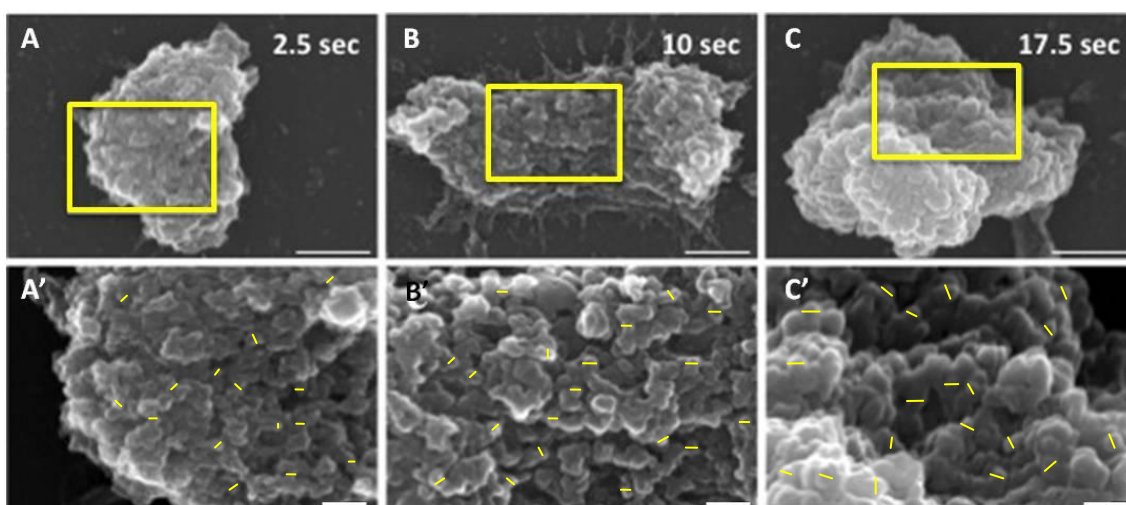


Figure 14. The longer coating times resulted in the larger chromatin diameter. Chromosomes were coated for 2.5 s (Figs. 14A, A'), 10 s (Figs. 14B, B'), and 17.5 s (Figs. 14C, C'). Yellow arrows illustrate the measurement of chromatin particles ( $n = 150-300$ ). Bars: 500 nm (A, B, C), 100 nm (A', B', C').

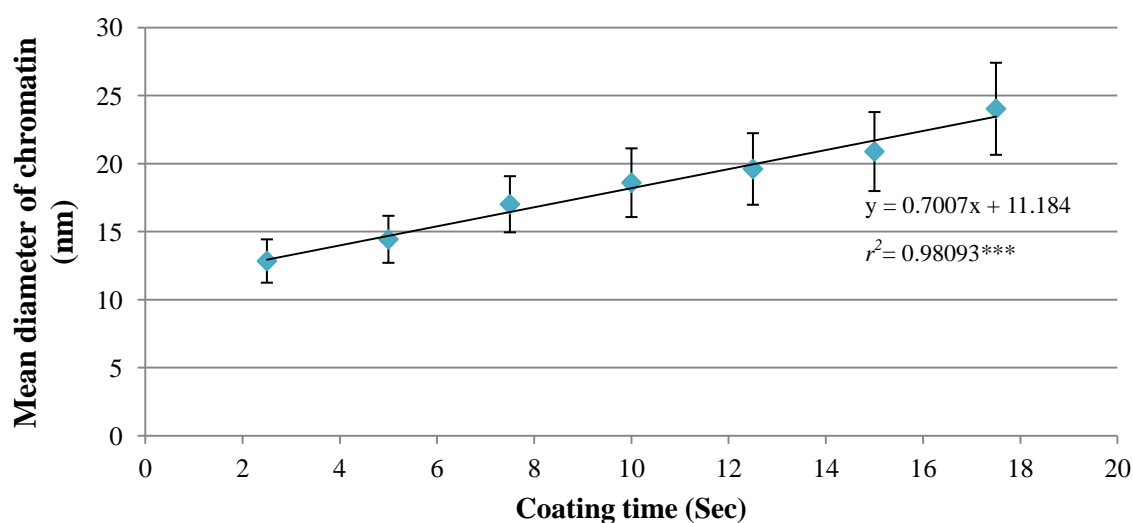


Figure 15. The linear increase of chromatin diameters (Fig. 14) according to the increase of coating time observed by SEM.

### 3.3.2 Uncoated chromosome visualization by HIM

Figures 16A and B show HIM images of an uncoated chromosome. It is evident that chromosomes can be visualized at high resolution even without metal/carbon coating. This chromosome was prepared with the buffer without  $\text{Mg}^{2+}$ , and showed a fibrous structure by HIM. The image was in high contrast and focused, and revealed detailed morphological information, including chromatin fibers with a diameter of 11 nm (Fig. 16B).

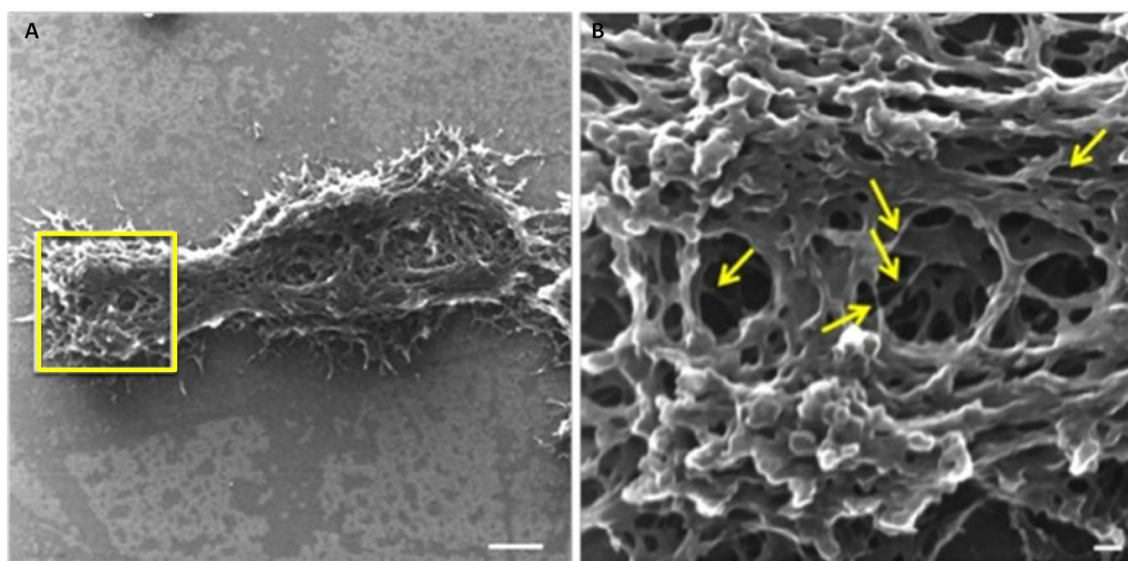


Figure 16. Chromosome could be visualized by HIM without metal coating. Yellow arrows indicate 11 nm fibers. Bars: 500 nm (A), 100 nm (B).

### 3.3.3 The effect of $\text{OsO}_4$ coating on chromosome structure visualized by HIM

To investigate the effect of  $\text{OsO}_4$  coating on chromosome structure, structure of coated and uncoated chromosomes was compared, as shown in Figures 17 and 18. Two different concentrations of  $\text{Mg}^{2+}$  (5 and 0 mM) were applied to the chromosomes. Figure 17 shows images of chromosomes treated with 5 mM  $\text{Mg}^{2+}$ . This concentration gave an overall globular and highly condensed chromosome structure with relatively smooth surfaces, both in uncoated (17A, 17A') and coated chromosomes (17B, 17B'). However, it is obvious that chromatin structural information could be obtained more clearly with

uncoated chromosome (Figs. 17A, A') than coated chromosome (Figs. 17B, B'). The mean diameter of the coated globular structures (Fig. 17B') was  $40.36 \pm 4.4$  nm (mean  $\pm$  SD, n = 50), compared to an uncoated mean diameter of  $31.73 \pm 3.9$  nm (Fig. 17A'). This difference might be caused by the OsO<sub>4</sub> coating covering the true surface structure of the chromosome.

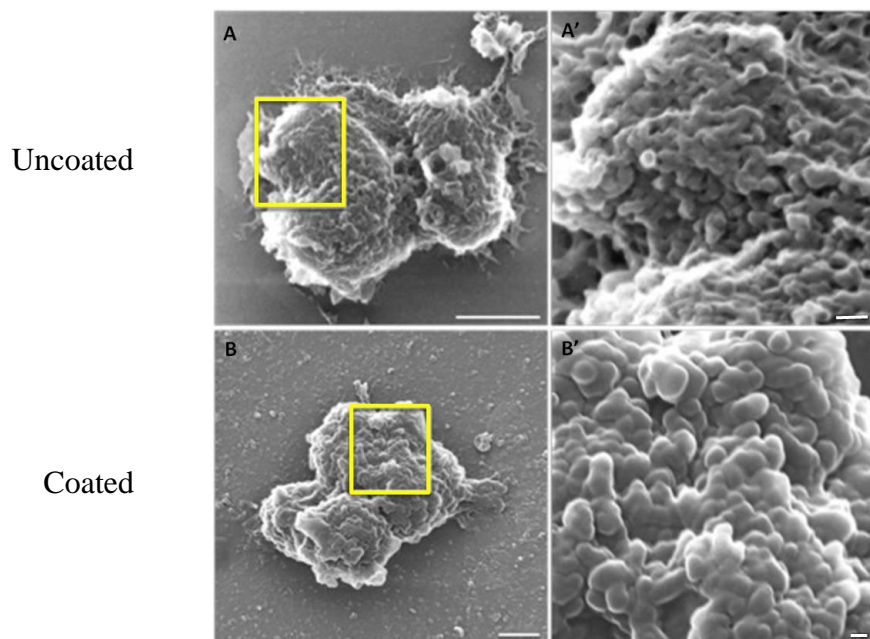


Figure 17. Uncoated chromosome (Fig. A, A') has smaller chromatin globular structure compared with the coated one (Fig. B, B'). Chromosomes were treated with 5 mM Mg<sup>2+</sup>. Bars: 500 nm (A, B), 50 nm (A', B').

Similar results are also seen in Figure 18 which shows chromosomes treated with buffer without Mg<sup>2+</sup>. Comparison between OsO<sub>4</sub>-uncoated (Figs. 18A, A') and coated (Figs. 18B, B') images taken by HIM clearly shows that the chromatin fibers in uncoated chromosomes appear more focused and have better contrast. The mean diameter of the chromatin fibers was  $11.17 \pm 2.9$  nm without coating and  $22.79 \pm 4.5$  nm after OsO<sub>4</sub> coating.

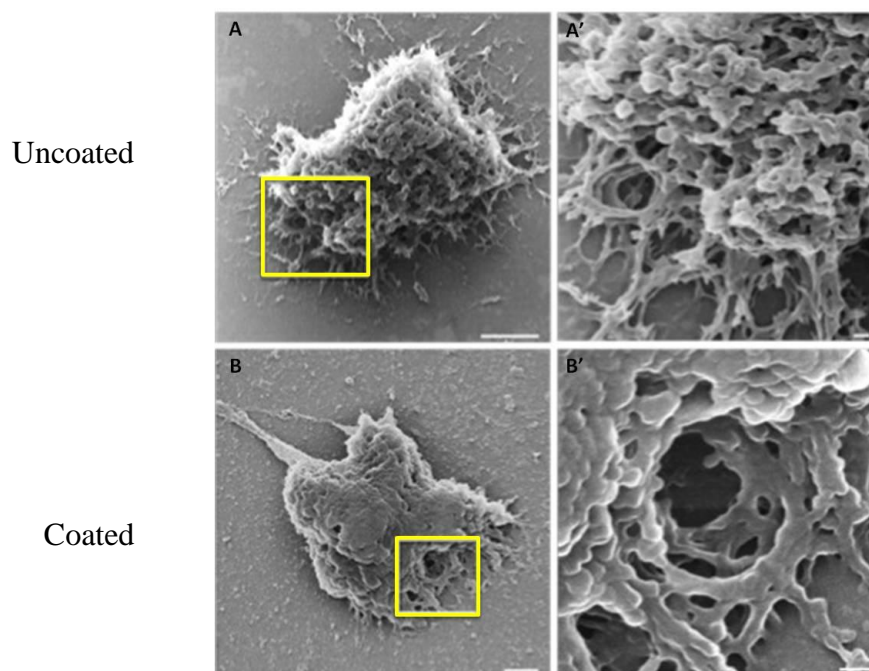


Figure 18. Uncoated chromosome (A, A') has smaller chromatin particles compared with the coated one (B, B'). Chromosomes were treated with 0 mM  $Mg^{2+}$ . Bars: 500 nm (A, B), 50 nm (A', B').

### 3.3.4 The effect of $Mg^{2+}$ on chromosome structure visualized by HIM

The different structure of uncoated chromosomes in different  $Mg^{2+}$  concentration was evaluated by HIM. The results revealed that chromosome treated with 0 mM  $Mg^{2+}$  showed a relatively less compact structure compared with those treated with 5 mM  $Mg^{2+}$  (Fig. 19).

Different mean diameters of chromatin depending on  $Mg^{2+}$  concentration and  $OsO_4$  coating treatment were revealed by HIM observation. Chromatin diameter was nearly 30 nm in the presence of 5 mM  $Mg^{2+}$  but show 11 nm fibers in the absence of  $Mg^{2+}$ . These results indicate that the degree of chromosome compaction and chromatin diameter vary with  $Mg^{2+}$  concentration. To summarize, the effect of  $Mg^{2+}$  and  $OsO_4$  coating was presented in Figure 20.

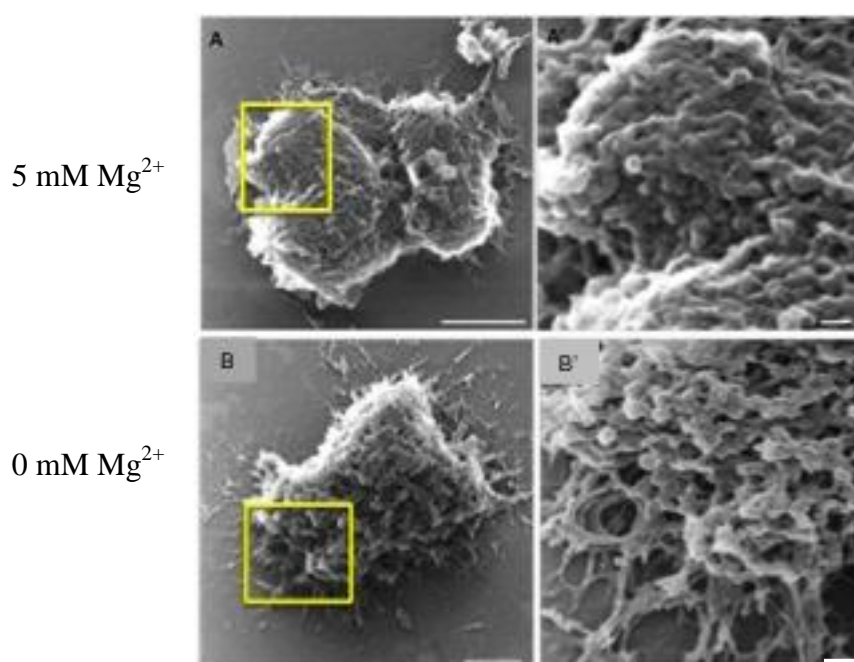


Figure 19. Chromosome treated with 5 mM  $Mg^{2+}$  showed compact structure with globular chromatin particles (A). The structure became more fibrous when the chromosome was treated with buffer containing no  $Mg^{2+}$  (B). Bars: 500 nm (A, B), 100 nm (A', B').

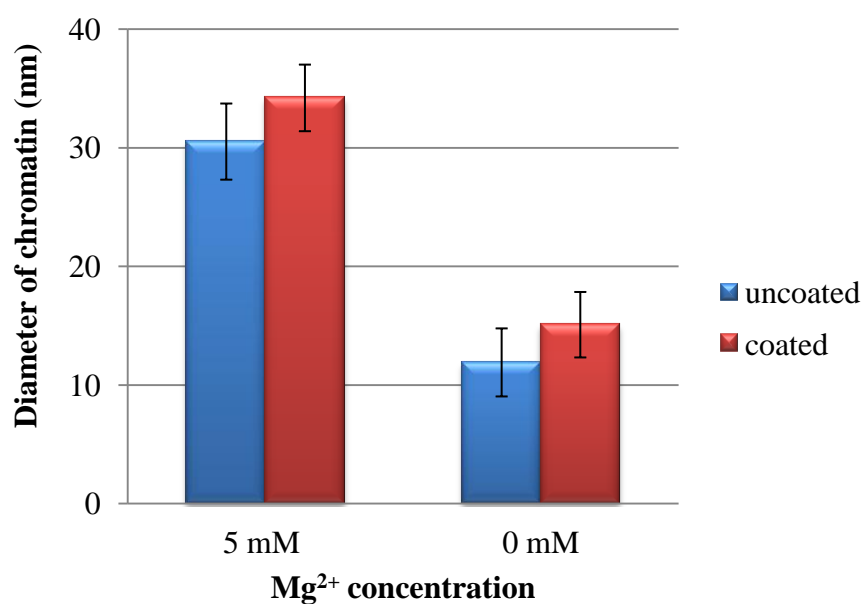


Figure 20. The effect of  $Mg^{2+}$  and  $OsO_4$  coating on chromatin mean diameter.



### 3.3.5 The effect of $Mg^{2+}$ on chromosome structure visualized by SEM and HIM

To finally evaluate the contrast and resolution advantage of HIM compared with SEM,  $OsO_4$ -coated chromosomes in different concentration of  $Mg^{2+}$  were observed by SEM and HIM.

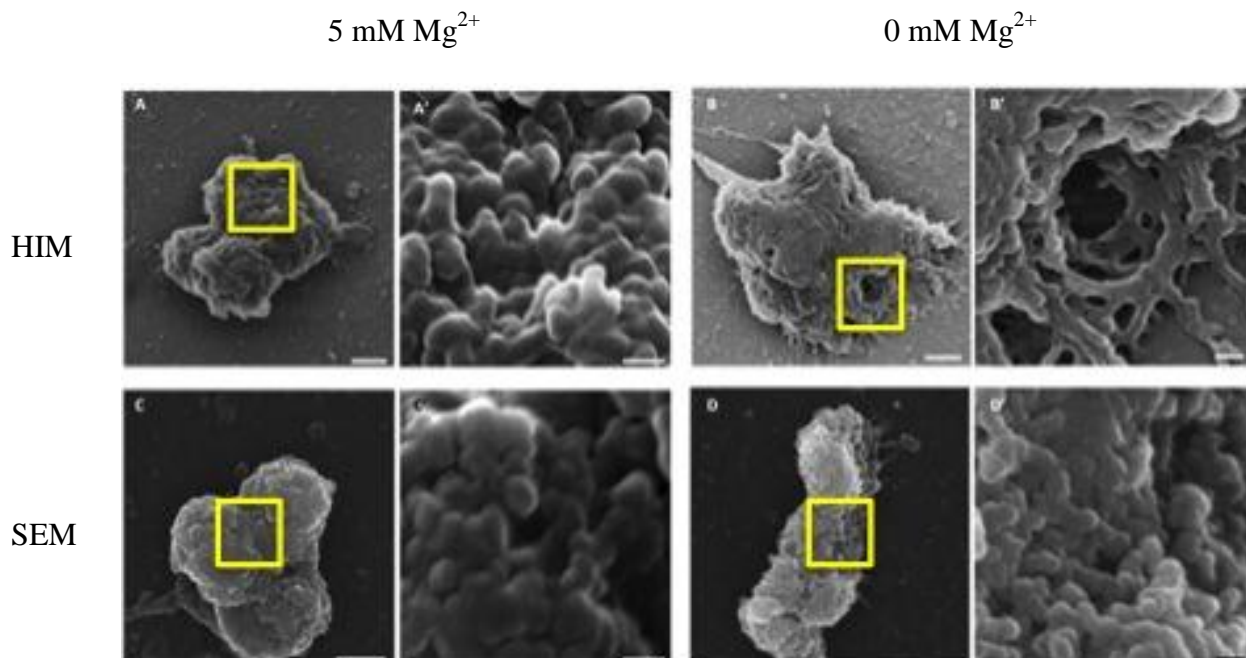


Figure 21. Higher contrast and resolution images were obtained by HIM compared with SEM. Chromosomes were treated with 5 mM (A, A', C, C') and 0 mM  $Mg^{2+}$  (B, B', D, D') and observed by HIM (A, A', B, B') or SEM (C, C', D, D'). Bars: 500 nm (A, B, C, D), 100 nm (A', B', C', D').

### 3.4 Discussion

SEM is a powerful tool for studying chromosome morphology, however being nonconductive, chromosomes require metal/carbon coating that may conceal information about the detailed surface structure of the sample. Visualization of uncoated chromosomes by SEM is impossible because they were heavily charged up during observation.

Osmium conductive metal coating is commonly performed for SEM observation of biological samples to avoid charging phenomena (Osawa & Nozaka, 1998; Suzuki, 2002; Shinaoka et al., 2013). However, based on the results, the mean diameter of chromatin

fibers was clearly increased by OsO<sub>4</sub> coating, and longer coating times resulted in thicker coating layers. OsO<sub>4</sub> coating may thus obscure the genuine and detailed structure of chromosomes. In addition, the thickness of the coating layer cannot be precisely regulated.

In this study the first HIM images of uncoated chromosomes in high resolution and contrast are reported, including the 11 nm chromatin fibers. Imaging of biological samples usually requires extensive processing. However, it has long been pointed out that the metal coating in sample preparation for SEM observation might induce artifacts leading to data misinterpretation.

In addition, the high contrast and resolution images from uncoated samples obtained by HIM enable investigation on the effects of Mg<sup>2+</sup> on chromosome structure. Chromatin fiber information was obtained more clearly with uncoated than coated chromosomes. Based on the results, the mean diameters of chromatin in chromosomes with an OsO<sub>4</sub> coating were 8-11 nm thicker than those without coating.

Effects of Mg<sup>2+</sup> concentration on the chromosome surface were also evaluated in this study. Differences in surface structure and chromatin diameter were clearly revealed. Treatment with 5 mM Mg<sup>2+</sup> showed highly condensed chromosomes with a largely uniform distribution of chromatin across and along the chromatid arms. Individual fibers could not be distinguished, even in uncoated chromosomes. When Mg<sup>2+</sup> was absent in the buffer (0 mM), chromosomes became less condensed and the diameter of the chromatin globular structure was smaller than those treated with 5 mM Mg<sup>2+</sup>. These results are in agreement with previous reports (Cole, 1967; Adolph et al., 1986; Caravaca et al., 2005).

Uncoated chromosomes could not be observed by SEM because of the charging phenomena caused by accumulation of negatively charged primary electrons. It is worth mentioning that the charge compensation system supplies negatively charged electrons



from a flood gun in HIM, which is effective enough that charge accumulation on the chromosome surface was suppressed to a negligible level in the HIM system. Detailed information, including 11 nm chromatin diameters, could be obtained from uncoated chromosomes observed by HIM, demonstrating both its high resolution and its advantages in avoiding artifacts caused by metal coating.

### **3.6 Summary**

In conclusion, it is shown that HIM imaging of uncoated chromosomes reveals the high resolution chromatin structure and overall chromosome surface structure without charging phenomena. HIM can provide a wealth of information over SEM because the atoms in HIM were formed as a trimer which has much smaller spot size and minimum surface interaction leading to the higher focus and resolution, reaching to 0.25 nm. In addition, this system is equipped with flood gun which generates electrons to neutralize the charge accumulation on the surface of the sample, enables biological sample observation without metal coating. These advantages of HIM make it an extremely promising tool in the field of life sciences. Based on the results, 30 nm globular structures could be visualized in uncoated chromosomes treated with 5 mM  $\text{Mg}^{2+}$ , and 11 nm structures were observed in the uncoated chromosome treated with buffer without  $\text{Mg}^{2+}$ . We conclude that HIM is a powerful tool for investigating chromosomes and other biological samples without requiring metal coating.

## **Chapter 4**

### **Chromosome observation by scanning electron microscopy using ionic liquid**

## 4.1 Introduction

IL has been used in a variety of fields because of its attractive features including high conductivity and negligible volatility. By considering its properties, IL can be used as an electron conducting material for biological sample preparation for SEM observation without dehydration, drying, and metal coating which have been inevitable for conventional preparation method and thought to be the major causes of artifacts production. By using this method, biological samples would maintain their condition closer to the native once. In addition, this newly developed method is also time-saving compared with conventional methods. Thus, the main objective of this study is to observe chromosome higher-order structure by SEM using IL method.

In this chapter, the study to reveal the effect of IL on chromosome structure has first been carried out by using HeLa cells as the samples. Then, the IL method was applied to visualize chromosomes. Spread chromosomes of Indian muntjac and human chromosomes were chosen for investigation because of their large size and low diploid number (5-14  $\mu\text{m}$  in length,  $2n = 6$  for female; 7 for male,) of Indian muntjac chromosomes (Wurster and Benirschke, 1970), and there being a well-established method for isolating the chromosomes from HeLa S3 cells for observation of chromosome higher-order structure (Uchiyama *et al.*, 2008; Ushiki *et al.*, 2008), respectively.

Some factors affecting the visualization of chromosome using IL by SEM were further optimized. The use of the hydrophilic imidazolium-based IL, EMI-BF<sub>4</sub> and BMI-BF<sub>4</sub>, in investigating chromosome higher-order structure was evaluated. In addition, the combination of IL with Pt-blue was also examined. Pt-blue has high affinity to DNA (Wanner and Formanek, 1995; Inaga *et al.*, 2007, Nishiyama, 2010).

## 4.2 Materials and Methods

### 4.2.1 Sample preparation

Indian muntjac cells were cultured in RPMI media supplemented with 10 % fetal calf serum. The spread chromosomes were prepared by synchronizing the cultured cells with 0.1 µg/mL colcemid (10 µL/mL) for 18 hrs at 37 °C to retrieve mitotic cells. Cells were collected by inverting the culture, and then centrifuged twice at 200 g and 25°C for 5 min (TOMY, MX-100).

Hypotonic treatment was carried out by incubating the suspension cells with 75 mM KCl for 15 min at 37°C. Chromosomes were spread onto ITO membrane (Indium Tin Oxide, Matsunami Glass Ind., Ltd.), Aluminum substrate, or OsO<sub>4</sub>-coated coverslips by centrifugation at 2,000 rpm for 10 min (Shandon Cytospin 4, Thermo). Spread chromosomes were then treated with 0.5% Triton X-100 (Sigma Aldrich) for 15 min, fixed with 2.5% (v/v) glutaraldehyde/PBS at room temperature for 30 min, and washed with Milli-Q water.

The isolation method of human chromosomes from synchronized HeLa S3 cells was carried out according to the method described previously by Uchiyama *et al.* (2004, 2005) and also Hayashihara *et al.* (2008). Human chromosomes were placed on the coverslips, incubated on ice for 10 min, fixed with 2.5% glutaraldehyde/PBS and 0.2% tannic acid/PBS at room temperature for 30 min, and washed with Milli-Q water.

For the evaluation of Mg<sup>2+</sup> effect on chromosome structure, chromosomes were treated with two different buffers XBE5 (5 mM Mg<sup>2+</sup>) and XBE (0 mM Mg<sup>2+</sup>) for 30 min, followed with 2.5% glutaraldehyde/XBE5 or 2.5% glutaraldehyde/XBE and 0.2% tannic acid/XBE5 or 0.2% tannic acid/XBE fixation, and finally washed with buffer prior to IL treatment.

#### **4.2.2 Ionic liquid pretreatment**

The EMI-BF<sub>4</sub> and BMI-BF<sub>4</sub> were purchased (MERCK). EMI-lactate was also purchased (Sigma Aldrich). IL was diluted to 0.1%, 0.5%, 1% and 3% with Milli-Q water, mixed by vortex for 1 min, and subsequently pre-warmed to 40°C prior to use.

#### **4.2.3 Ionic liquid treatment**

Chromosomes were treated with IL for 1 min at room temperature. The excess IL was absorbed by paper towels (KimWipes). Samples were then dried in the vacuum pumping system for 1 hr, and were directly observed by SEM or HIM.

#### **4.2.4 SEM observation**

Chromosomes were observed by low vacuum SEM (HITACHI, S-3500N) and high vacuum SEM (HITACHI, S-5200) with the electron voltage of 1.5-10 kV in secondary electron (SE) mode. For investigating the effect of platinum blue (Pt-blue) staining (TI blue, Nisshin EM Corporation) combined with IL, chromosomes were treated with Pt-blue for 15 min prior to IL treatment.

#### **4.2.5 HIM observation**

Chromosomes prepared with IL method were observed by HIM (Orion Plus, Zeiss, Oberkochen, Germany) with an accelerating voltage of 30 kV, a beam current of 6.8 pA, and working distance of 6.4 mm.

### **4.3 Results**

#### **4.3.1 Preliminary experiment**

To check the effect of IL, chromosomes treated with IL were preliminarily observed

by FM. The result showed no significant difference between the morphological structures of chromosomes with and without IL treatment (Fig. 22). These results suggest that IL does not cover the chromosome structure completely. The contour of chromosome could be defined including centromere and chromosome arms.

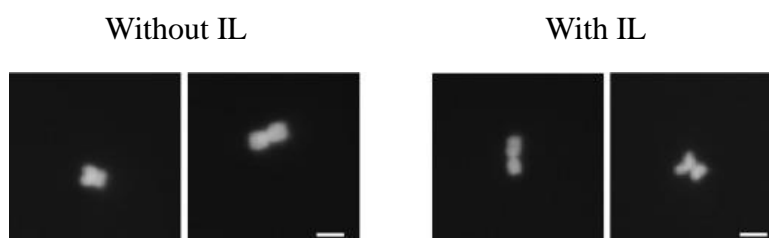


Figure 22. Chromosomes with and without IL showed similar structure observed by optical microscope. Bars: 1  $\mu\text{m}$ .

Furthermore, to investigate the applicability of IL for SEM observation, HeLa cells were preliminarily chosen as the samples due to its larger size than the chromosome. The results showed that HeLa cells could be visualized by low vacuum SEM for the first time without dehydration, drying, and metal coating after they were treated by EMI-lactate as shown in Figure 23.

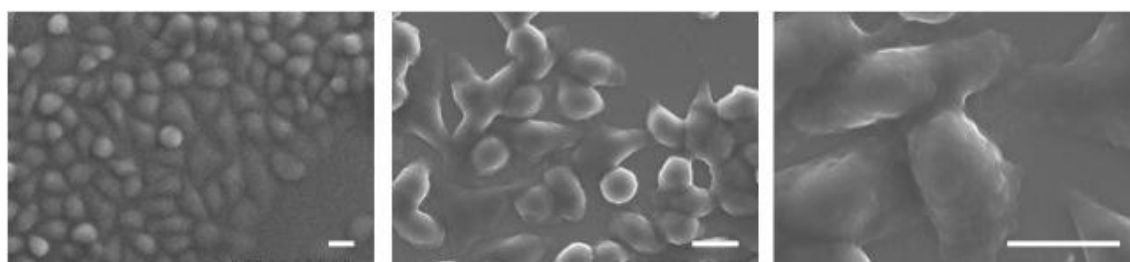


Figure 23. HeLa cells images after EMI-lactate treatment by SEM. Bars: 10  $\mu\text{m}$ .

Two kinds of IL were then investigated for observing HeLa cells. Fine external structures of HeLa cells were clearly observed after treated by EMI-BF<sub>4</sub> compared with those treated by EMI-lactate (Fig. 24). It was also found that pretreatment of the IL by warming and mixing processes efficiently enhanced the resolution and the contrast of scanning electron micrographs. Such pretreatment reduces the viscosity of the IL,

avoiding the concentration of IL in a limited area.

In order to optimize the concentration of IL for visualizing chromosome higher-order structure, IL was diluted with Milli-Q water to decrease concentrations prior to applying them to the chromosomes, since their high viscosities result in the IL pooling, which may disturb chromosome visualization by SEM. The observation of chromosome prepared with IL method was optimum at lower concentrations of IL (0.5-1%).

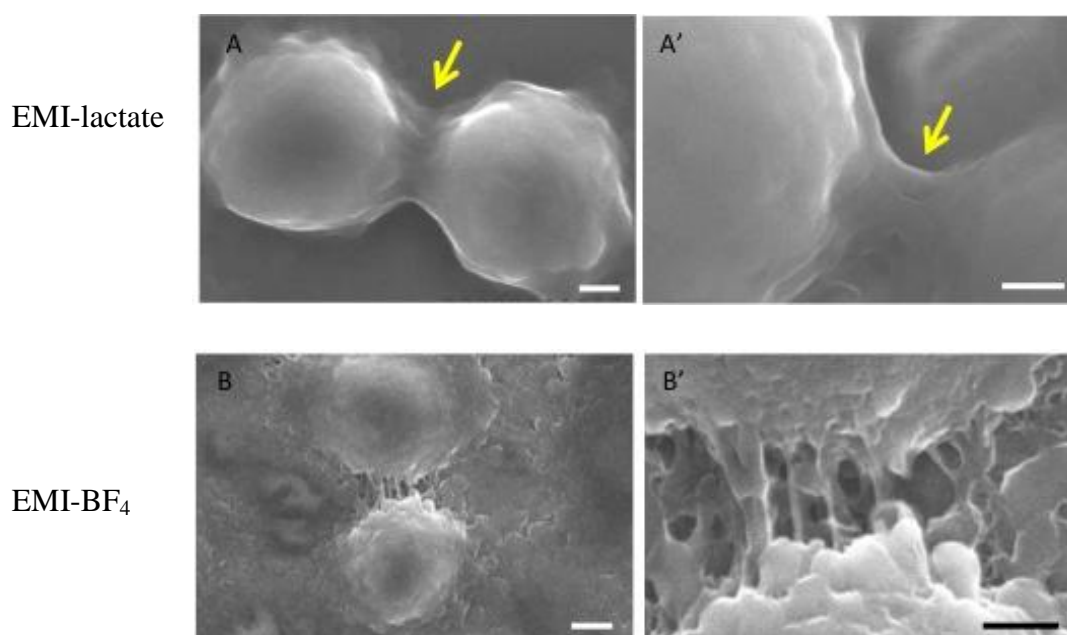


Figure 24. HeLa cells images after EMI-lactate (A, A') and EMI-BF<sub>4</sub> (B, B') treatment as observed by low vacuum SEM. Yellow arrows show the excess of IL which hide the surface structure of HeLa cell. Bars: 1 μm (A, A', B'), 2 μm (B).

#### 4.3.2 Chromosome observation after IL treatment

Spread chromosomes on ITO-coated coverslips treated with 0.5 or 1.0% EMI-BF<sub>4</sub> were observed by low vacuum SEM (Figs. 25A-D). The results showed that the chromosomes with the length of  $\pm 5 \mu\text{m}$  prepared with those IL concentrations could be observed by SEM using IL method, without dehydration and metal coating. The chromosome contours were sharply defined (Figs. 25A, B), and the fibers between

individual chromosomes were visible (Figs. 25C, D). However, these micrographs did not show any three-dimensional appearance of the chromosome structure, and the details of the chromatin fiber could not be observed due to the limited resolution.

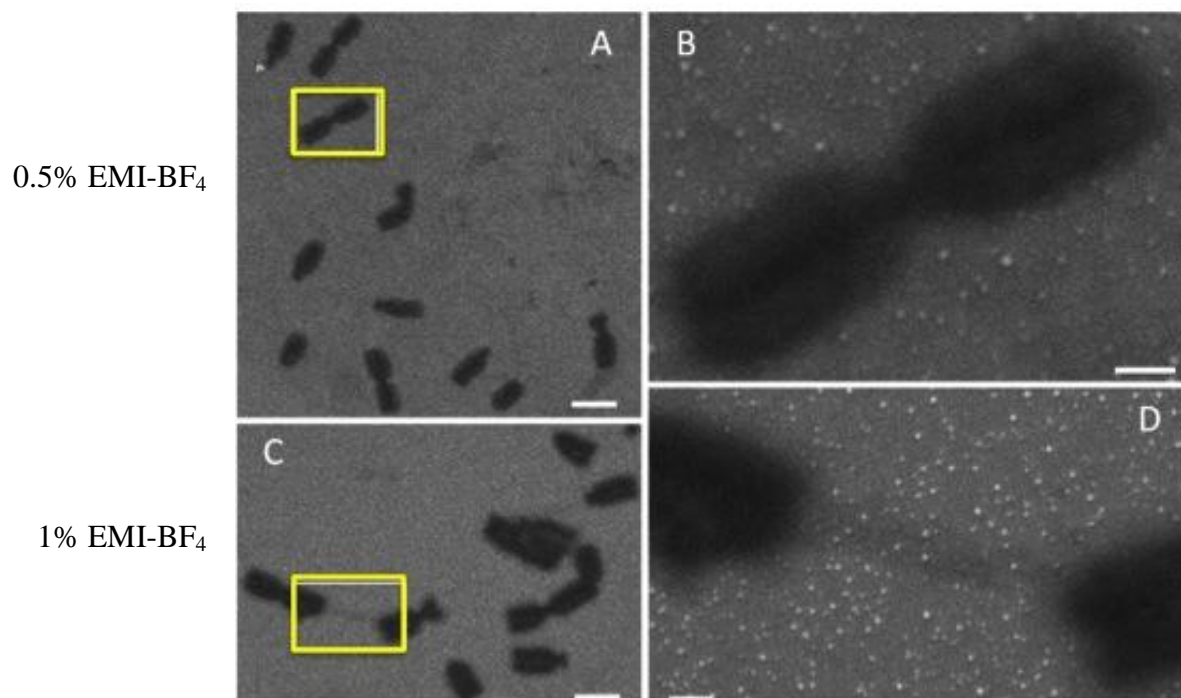


Figure 25. Spread chromosomes visualized after IL treatment. Chromosomes were treated with 0.5% EMI-BF<sub>4</sub> (A, B) and 1.0% EMI-BF<sub>4</sub> (C, D). Bars: 5  $\mu$ m (A, C), and 1  $\mu$ m (B, D).

To get the better resolution, the samples were then observed by ultra-high resolution SEM (S-5200). As a result, chromosome images showed good contrast and relatively clear contour features compared with those observed by low vacuum SEM (Figs. 26).



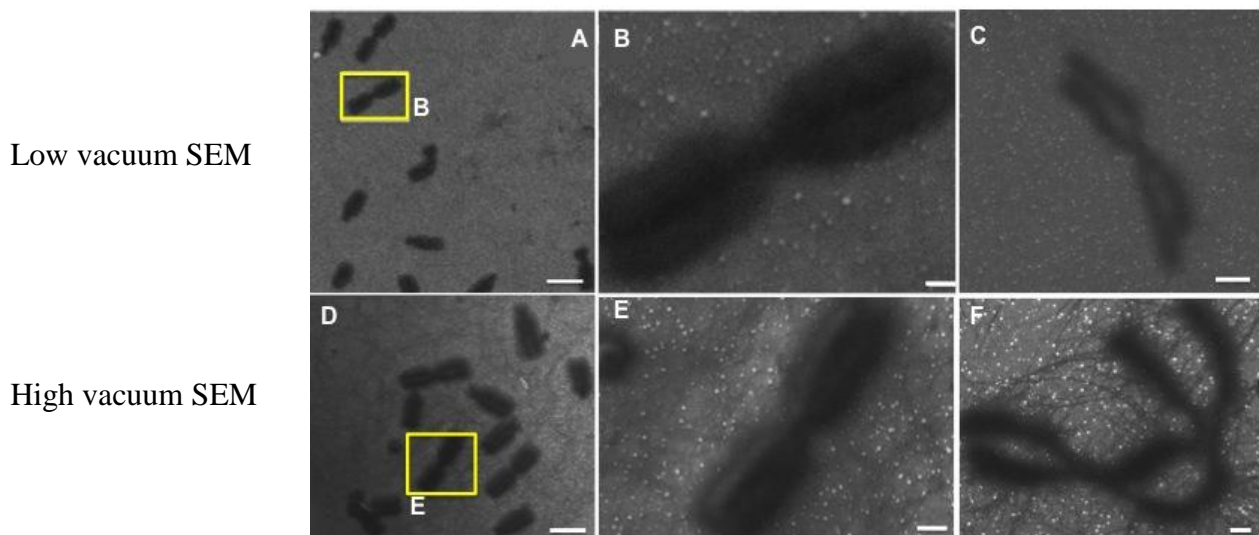


Figure 26. The IL-treated chromosomes observed by low (A, B, C) and high vacuum SEM (D, E, F). Bars : 5  $\mu\text{m}$  (A, D), 1  $\mu\text{m}$  (B, C, E, F).

In order to further enhance the electron conductivity of the chromosomes, Pt-blue was applied before the IL treatment. The results revealed that the addition of Pt-blue enhanced the contrast of chromosomes, enabling visualization of three-dimensional and bumpy surface structures even by low vacuum SEM (Fig. 27).

After Pt-blue staining, the chromosomes were treated with 0.5% or 3% EMI-BF<sub>4</sub>. Chromosomes treated with 0.5% EMI-BF<sub>4</sub> gave higher resolution images with detailed surface structures (Fig. 27A, B) than those treated with 3% EMI-BF<sub>4</sub>, which showed a smoother surface (Fig. 27C, D). In the higher magnification (Fig. 27D) the chromosome treated with 3% EMI-BF<sub>4</sub> was shown in the blurry image. These results indicated that the higher concentration of IL resulted in IL pooling on the chromosome surface, which interferes with visualization of constructional details, probably due to the scattering of electron beam by the liquid (Kuwabata *et al.*, 2011). Therefore, further studies on human chromosomes were conducting using lower concentrations of IL (0.5-1%).

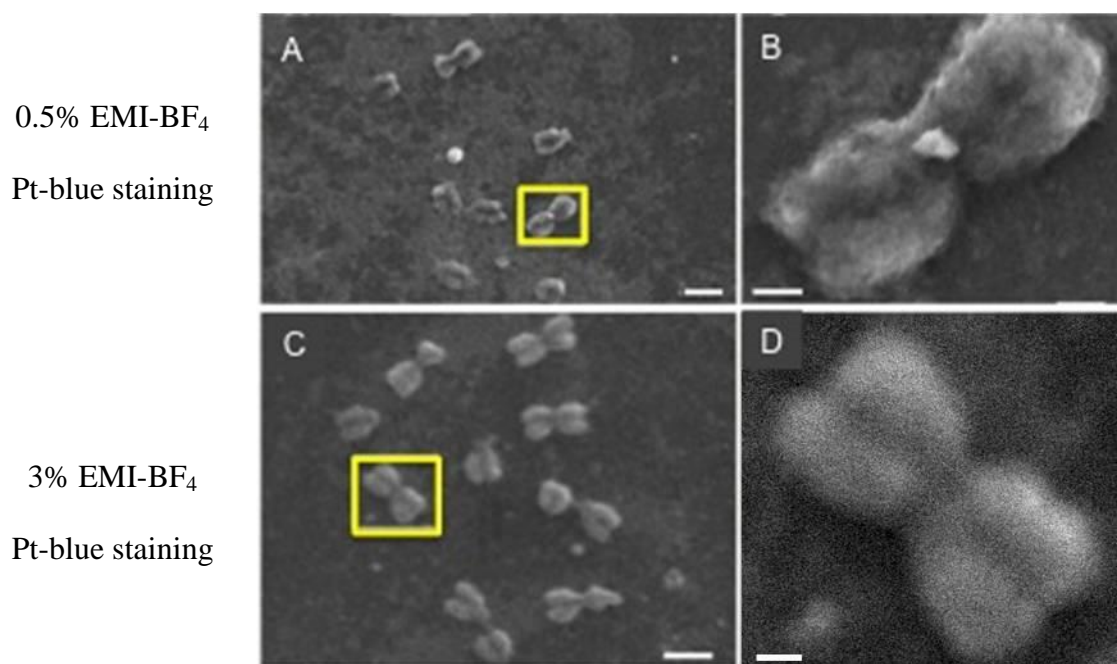


Figure 27. The contrast of IL-treated chromosomes can be enhanced by applying Pt-blue treatment and using lower concentration of IL. Higher magnification image of chromosome treated with 0.5% EMI-BF<sub>4</sub> (B) showed higher contrast compared with those treated with 3% EMI-BF<sub>4</sub> (D). Bars: 5  $\mu$ m (A) and 1  $\mu$ m (B, D).

High concentration resulted in appearance of some IL pools on surfaces of some cells. This may be due to relatively high viscosity of IL on the specimen. On the other hand, choice of lower IL concentrations caused easy charge-up of the cells even at lower accelerating voltages (Ishigaki *et al.*, 2011).

#### 4.3.3 Chromosomes stained with Pt-blue and prepared with IL

The EMI-BF<sub>4</sub> and BMI-BF<sub>4</sub> were applied on the chromosomes and observed by SEM (Fig. 28). After Pt-blue staining, chromosome images showed the better resolution and higher contrast. In addition, these results also show that BMI-BF<sub>4</sub> is more suitable for chromosome observation by SEM compared with EMI-BF<sub>4</sub>.

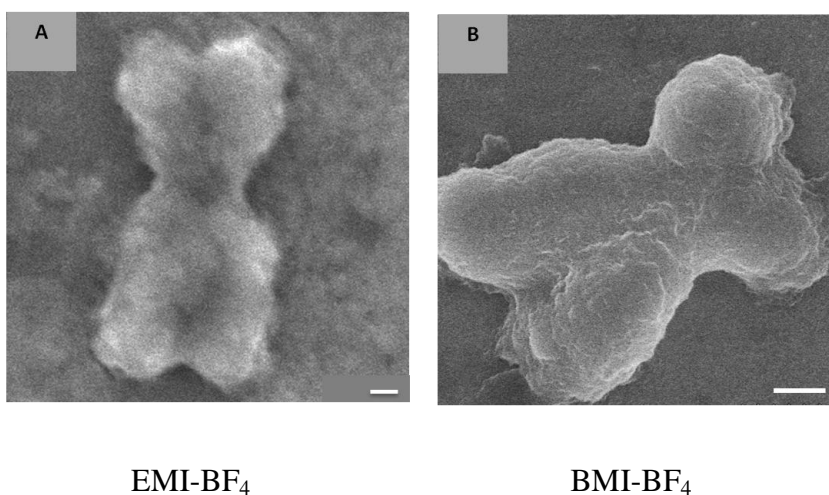


Figure 28. Chromosome treated with BMI-BF<sub>4</sub> (B) showed better resolution and contrast compared with that of EMI-BF<sub>4</sub> (A). Bars: 1  $\mu$ m (A, C), 250 nm (B, D).

To finally evaluate the advantage of IL method, chromosomes prepared with conventional and IL methods were compared by performing SEM observation. Conventional method includes dehydration, drying, and metal coating steps with the total preparation steps of 7-8 hours. In contrast, IL method takes only 50 min. However, as shown in Figure 29, chromosomes prepared with both methods presenting the similar resolution. This result clearly indicates that IL method is superior not only in term of maintaining the structure close to the native but also in time saving.

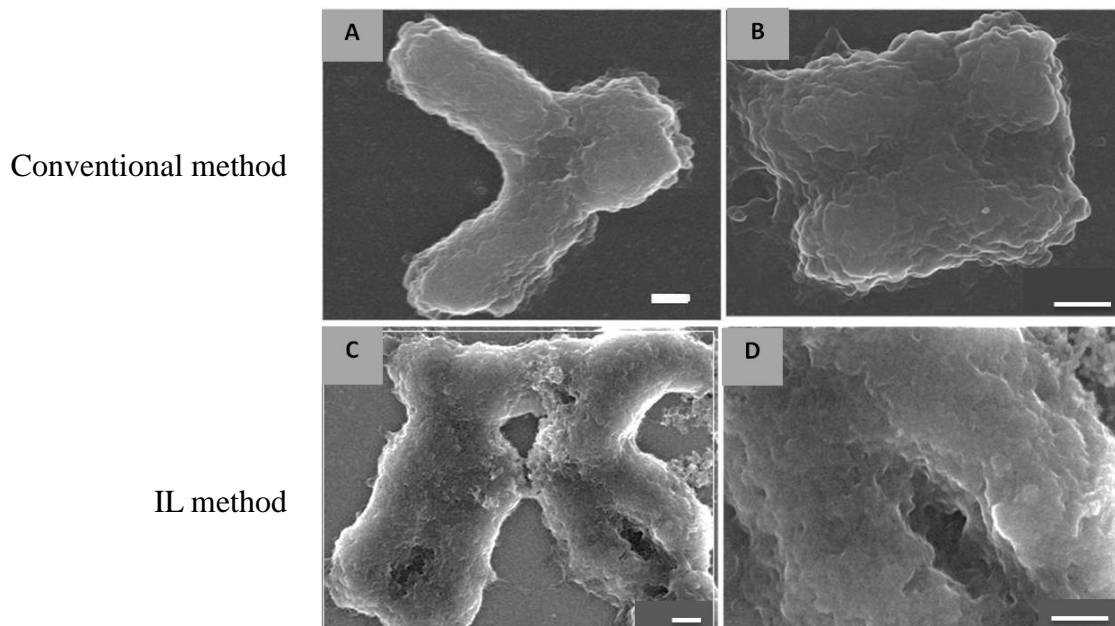


Figure 29. Chromosome prepared with conventional method (A, B), and IL method (C, D) showed the similar resolution images observed by SEM. Bars: 250 nm.

#### 4.3.4 The effect of $Mg^{2+}$ on IL-treated chromosome structure observed by SEM

As described above, the IL method has now been proven to be applicable for chromosome observation by SEM. Some parameters related to its applications for chromosome observations including the type and concentration have also been optimized. The exploration of this new method to study the chromosome structure was then further examined, specifically with regards to the effect of  $Mg^{2+}$ .

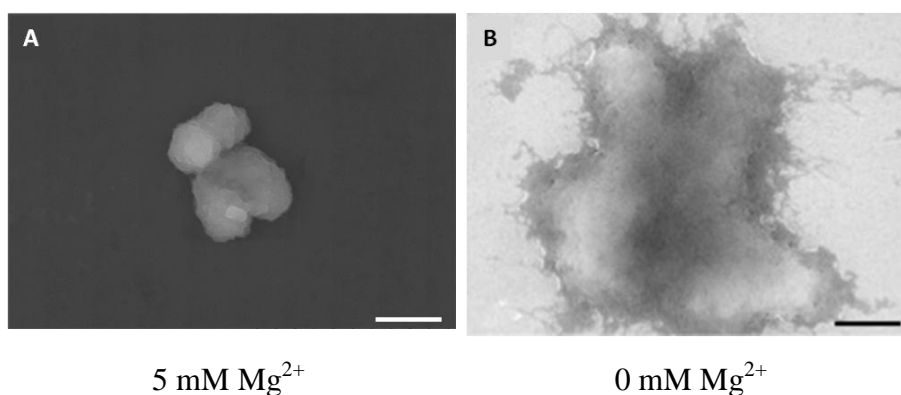


Figure 30. The different structure of chromosome in different  $Mg^{2+}$  concentration, 5 mM (A), and 0 mM (B), could be observed by SEM in rapid preparation by using IL method. Bars: 1  $\mu$ m.

Figure 30 indicates the different structure of chromosome morphology in different concentration of  $Mg^{2+}$ . Chromosome showed compact structure without any fibers radiated when it was treated with 5 mM  $Mg^{2+}$ . This compact structure, however, turned to be more expanded and dispersed with thin fibers radiated when the  $Mg^{2+}$  was absent.

#### 4.3.5 Higher resolution chromosome images by combining IL method and HIM

Having optimum conditions determined, the IL method was then explored further by applying it to the HIM for obtaining the higher resolution images. As described in the previous chapter, HIM has the advantage over SEM particularly in providing higher resolution reaching to 0.25 nm. The results showed that the higher resolution of chromosome images could successfully be obtained by combining the IL method with HIM. Chromosome images observed by HIM showed the higher resolution and stronger contrast compared with those obtained by SEM (Fig. 31).

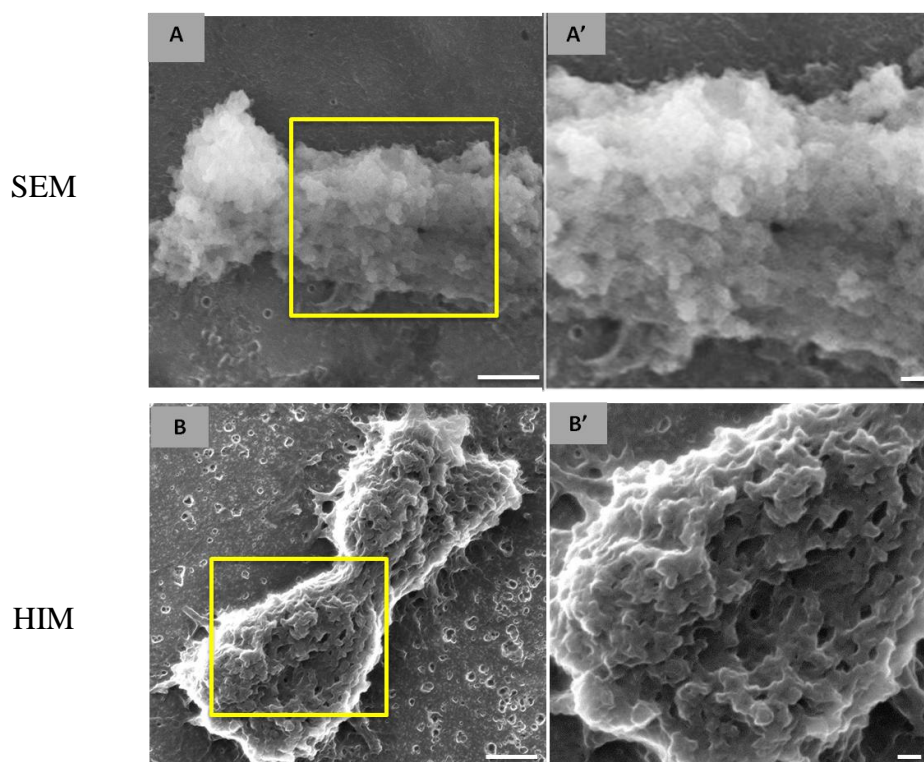


Figure 31. HIM observation (A, A') of chromosome prepared with IL method yields the higher resolution and stronger contrast compared with SEM observation (B, B'). Bars: 500 nm (A, B), 100 nm (A', B').

To get clearer illustration about the advantages of IL method, chromosome without coating, coated with OsO<sub>4</sub>, and prepared with IL method were observed by HIM which enabled uncoated chromosome observation and the results were compared as shown in Figure 32. The results implied that metal coating yields in the more compact structure with larger and overlapping chromatin particles hiding the roughness of the chromosome surface structure (Fig. 32B) as compared with the uncoated one (Fig. 32A). These chromosomes were subjected to the same concentration of Mg<sup>2+</sup> (0 mM) which supposed to give a less compact and more dispersed structure as shown by the uncoated one. The less compact structure could not be visualized in Figure 32B probably caused by the OsO<sub>4</sub> coating which covers the surface of the chromosome. The chromosome prepared with IL method (Fig. 32C), however, showed the similar structural morphology as compared with the uncoated one, suggesting that the IL does not change the morphology and hides the roughness of chromosome structure, rather showed the closer condition to its native status, without any covering material.

Furthermore, the global structure of chromosome prepared with IL method (Fig.32C) showed the more bumpy structure with adequate thickness compared with the uncoated chromosome prepared with conventional method (Fig. 32A), demonstrating the advantage of IL method in maintaining the condition of chromosome by avoiding dehydration and drying which can result in the shrinkage as previously been reported (Boyde and Macconachie, 1979).

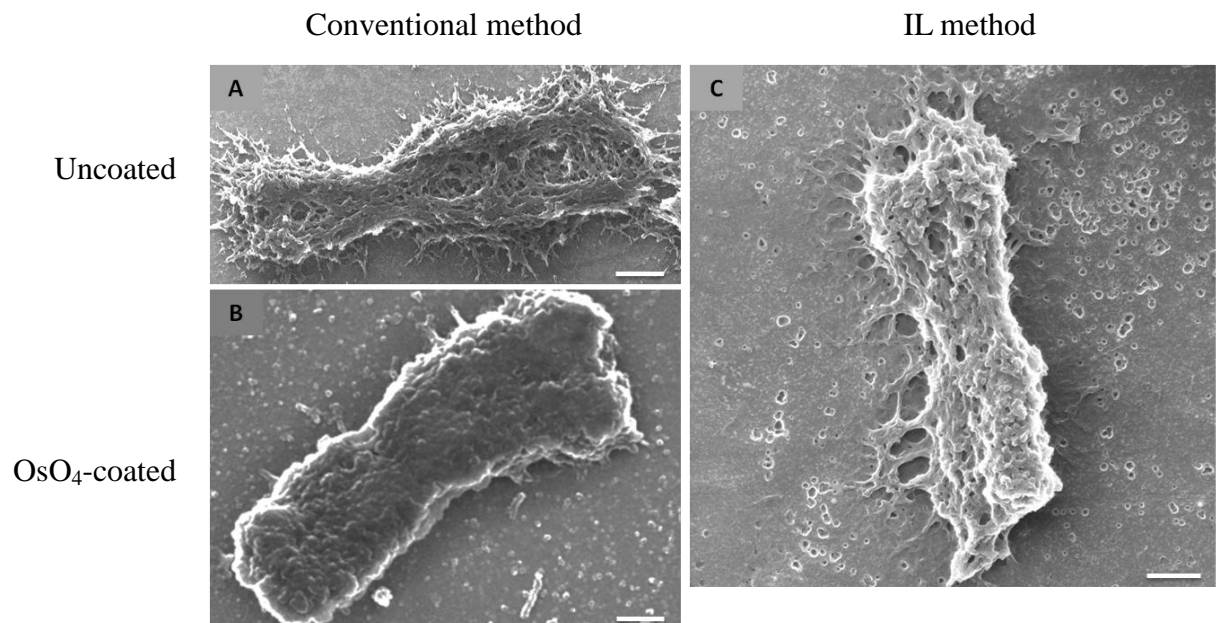


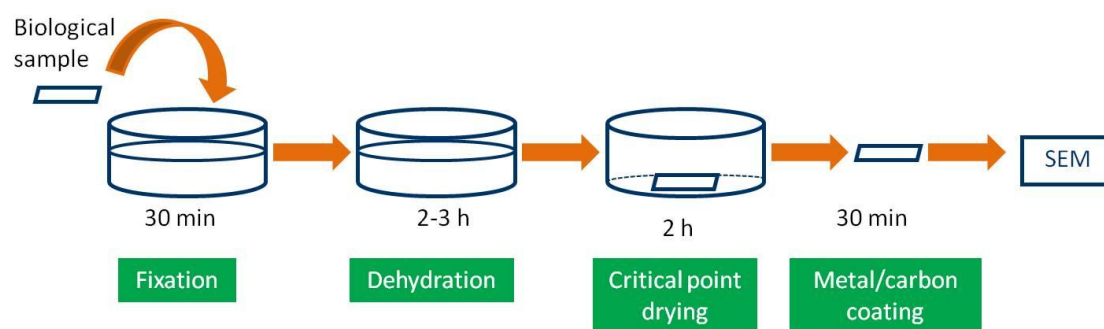
Figure 32. Chromosome prepared with IL method (C) showed the closer structural image with the uncoated one (A) as compared with chromosome coated with OsO<sub>4</sub> (B) observed by HIM. Bars: 500 nm.

#### 4.5 Discussion

Since biological samples must be inserted into the vacuum chamber inside electron microscope, wet specimens formerly had to be dried before observation. The dehydration and drying process have been reported to be the causes of shrinkage and artifact production. Furthermore, to give the electron conductivity, biological samples need to be coated by metal such as OsO<sub>4</sub>. However metal coating for biological samples is not preferable as this method cover the surface of the samples and therefore produces a false surface morphology (Pretorius, 2011). The finding that IL behaves like electronic conducting material has led to the utilization of IL for biological samples observation by EM. The scheme of conventional sample preparation method and IL method for SEM is briefly described in Figure 33.



### Conventional method



### Ionic liquid method

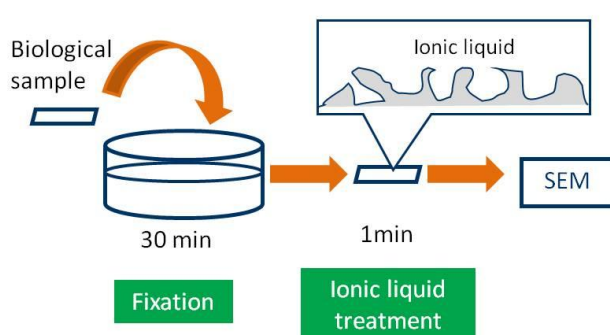


Figure 33. The schemes of conventional sample preparation and IL methods for SEM.

In this study the application of IL method for chromosome observation was evaluated and the results showed that chromosome higher-order structure could be visualized by SEM using the IL method without drying, dehydration, and metal coating. Some factors which affect chromosome visualization using IL method have also been investigated. Pre-warmed, well-mixed, and low concentration (0.5-1.0%) ILs provide well-contrasted images, especially when using BMI-BF<sub>4</sub>. Image contrast and resolution could be enhanced by the combination of IL and Pt-blue staining.

The most prominent characteristic of the IL method is its very short time course. The IL treatment after the fixation procedure takes only 1 min, which is a sharp contrast to the conventional method generally requiring 7-8 h. This implies that the IL method is the most rapid and simplest method for SEM analysis. In addition, this method requires no special equipment.



## 4.5 Summary

The development of IL method for chromosome observation by SEM, and also the factors affecting the visualization of chromosome observation by SEM were investigated. The results show that higher-order structure of chromosomes can clearly be visualized by applying the IL method without any dehydration, critical point drying or metal coating. Compared with conventional methods, this is a quick and efficient way to study chromosome higher-order structure by SEM. Other enhancements to obtain clearer images can be done by combining IL with Pt-blue, and the use of low concentration (0.5-1%) BMI-BF<sub>4</sub>. The exploration of the IL method to get higher resolution has successfully been carried out by combining it with the HIM system.

## **Chapter 5**

### **Chromosome interior investigation by FIB/SEM with ionic liquid**

## 5.1 Introduction

In the previous chapter, it is shown that the IL method is beneficial for chromosome observation by SEM without dehydration, drying, and coating, because IL behaves as the electronically conducting material in the electron microscopy. In this chapter, the interior of chromosome prepared both with the conventional and IL method were evaluated by using FIB/SEM, since there have been very few reports concerning chromosome interiors.

In FIB/SEM, the gallium ( $\text{Ga}^+$ ) primary ion beam will hit the sample surface and sputters a small amount of material. At low primary beam currents, FIB systems can be used for imaging. Furthermore, at higher primary currents, a great deal of material can be removed by sputtering, allowing precision milling of the specimen down to a sub micrometer or even a nano scale.

It has been shown that FIB/SEM dual beam apparatus makes *in situ* imaging of sample cross-sections possible in well-defined areas and gives a new insight into chromosome study (Schroeder-Reiter *et al.*, 2009, 2012). A cavity network in the chromosome interior was revealed. These results may reflect disruption of the proper arrangements of chromosome scaffold proteins that are distributed alternately along the axis of metaphase chromatids as shown by Ono *et al.*, (2004). Thus, it is an open question whether cavities might interfere with the distribution of scaffold proteins.

Ordinarily, biological sample preparation for SEM requires sequential steps, including dehydration, drying by critical point dryer (CPD), and metal coating. CPD is a commonly used method for biological sample drying. It relies on this physical principle. The water in biological tissue is replaced with a suitable inert fluid whose critical temperature for a realizable pressure is just above ambient. The choice of fluids is severely limited and  $\text{CO}_2$  is universally used

However, CPD may cause shrinkage under certain conditions (Boyde and Maconnachie, 1979, 1981; Boyde and Boyde, 1980). Furthermore, traces of water or ethanol may remain during CPD, and can distort ultrastructure and induce artifacts as has been shown by Ris (1985). Therefore, the establishment of a method that provides a sample condition closer to the native state by avoiding drying would be a powerful aid to investigating biological samples such as chromosomes by SEM.

As mentioned in the previous chapter, it is shown that the IL method is useful for the rapid preparation of chromosome samples for SEM. In addition, Pt-blue staining enhanced the contrast of chromosome images. By considering the advantages of the IL method with Pt-blue staining and FIB/SEM investigation, a combination of these two approaches should be appropriate to study the interior of chromosome. Herein the FIB/SEM observation of barley and human chromosomes is reported.

To get further insight into chromosome three-dimensional (3D) structure, and to confirm the results of FIB/SEM data, the IL method was also explored by taking the advantages of STEM tomography. This system is coupled with dark field and bright field detectors, allowing both topographical and compositional detections. By using STEM tomography, chromosome in 3D could be observed without sectioning.

## **5.2 Materials and Methods**

### **5.2.1 Barley chromosome preparation**

Barley seeds (*Hordeum vulgare*  $2n = 14$ , given by Prof. N. Ohmido, Kobe University) were germinated at 22°C in the dark on moist filter papers for 24-48 h until the root tips reached to 0.5-1 cm. The root tips were then cut off and stored in ice water for 24 h. After that, they were fixed in ethanol:acetic acid (3:1, v:v) for 24 h, washed for 30 min, and subjected to an enzymatic treatment consisting of 2.5 % Cellulase Onozuka RS (Yakult

Co., Tokyo, Japan), 2.5 % Pectolyase Y-23 (Kikkoman, Tokyo, Japan), and 75 mM KCl, pH 4.0 at 37 °C for 1-2 h. The root tips were subsequently put on aluminum foil, and excess water was removed by blotting paper. Chromosomes were spread by pinching the root tips with the addition of ethanol:acetic acid (3:1, v:v). For sample preparation for SEM, 2.5 % (v/v) glutaraldehyde/PBS and 0.2 % tannic acid/PBS were added immediately followed by incubation at room temperature for 30 min or at 4 °C overnight.

### **5.2.2 Human chromosome preparation**

Human chromosomes were isolated from HeLa S3 cells by the polyamine method (PA chromosomes, Hayashihara *et al.*, 2008) and were stored either in glycerol (-20° C) or PA buffer (150 mM Tris, 2 mM spermine, 5 mM spermidine, 20 mM EDTA/Na, 800 mM KCl, 1 M DTT, 30% empigen, 100 mM PMSF, 4° C). They were placed on aluminum foil on ice for 10 min, washed either with Sol. IV (5 mM Tris-HCl, 20 mM KCl, 10 mM EDTA-KOH, 0.25 mM spermidine, 1 % thiodiglycol, 0.1 mM PMSF, 0.05 % empigen) or XBE2 (10 mM HEPES, pH 7.7, 2 mM MgCl<sub>2</sub>, 100 mM KCl, 5 mM EGTA) for 5 min, followed by fixation with 2.5 % glutaraldehyde/XBE2 and 0.2 % tannic acid/XBE2 for 30 min at room temperature. Samples were then washed with XBE2 three times for 5 min each and subsequently treated either with IL or CPD as follows.

### **5.2.3 Ionic liquid treatment and critical point drying**

The 0.5 % BMI-BF<sub>4</sub> was prepared as described previously (Dwiranti *et al.*, 2012). Both barley and human chromosomes were treated with the IL by dropping 50 µL aliquots directly on the samples and incubated for 1 min at room temperature. The excess IL was removed by a blower followed by drying in a desiccator with vacuum pumping for 1 h. Pt-blue staining was performed prior to IL treatment for 15 min (pH = 9). The

samples were dissected/observed directly by FIB/SEM without ethanol dehydration, drying, or metal coating.

For chromosomes prepared with conventional method (CPD), samples were washed three times with XBE2 or PBS after fixation, followed by 2 % OsO<sub>4</sub> post-fixation, and washed again three times, 5 min each. Dehydration was carried out by using an ethanol series (70, 100, 100 %). Chromosomes were then dried by critical point dryer that was manually adjusted from one experiment to the next using 3-methylbutyl acetate, four samples per run, followed by OsO<sub>4</sub> coating, and finally dissected/observed by FIB/SEM.

#### **5.2.4 Sectioning and observation by FIB/SEM**

Aluminum foil with attached chromosome samples was cut to size, and mounted onto an aluminum stub. Chromosomes were dissected either by FIB (Seiko SMI-3050, SII Nanotechnology, Tokyo, Japan) or by the integrated FIB/SEM system (AURIGA 60, Zeiss, Oberkochen, Germany). The FIB uses Ga<sup>+</sup> accelerated by 30.0 kV. The FIB column was set at an angle of 54° in an AURIGA 60 system chamber. After sectioning, chromosomes were imaged by SEM (JEOL JSM-7600F, Tokyo, Japan). Some samples were observed by the integrated FIB/SEM system (AURIGA 60) at a working distance of 5.0 mm (2 nm resolution). Images were taken with various detectors as summarized in Table 2 and were divided into two general observation modes, secondary electron (SE) and back-scattered electron (BSE). SE detection provides the topographical information, while BSE detection is strongly correlated to the atomic composition (number, *Z*) of the specimen. A schematic representation of the FIB/SEM setup is presented in Figure 34.

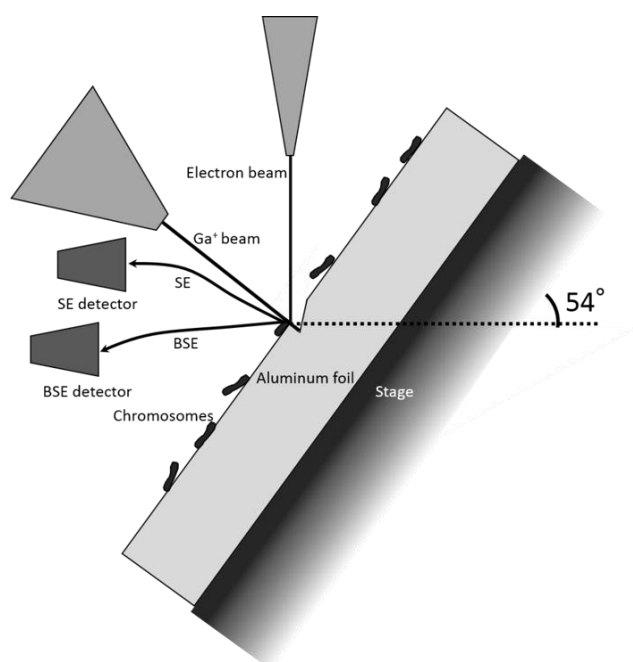


Figure 34. Schematic diagram of FIB/SEM. The stage is tilted at 54°, and the Ga<sup>+</sup> beam is irradiated from just above the chromosomes.

#### 5.2.5 Chromosome 3D visualization by STEM tomography

After IL treatment, chromosomes on the grids were directly observed by STEM without coating or any other preparation steps. Tilting series were recorded at  $\pm 60^\circ$  with the increment of  $2^\circ$ . The data were then aligned and analyzed by using IMOD software.

### 5.3 Results

Barley and human chromosomes were selected for the investigation due to their well-established preparation methods (Fukui and Kakeda, 1991; Uchiyama *et al.*, 2008; Hayashihara *et al.*, 2008). Preparation of chromosome samples included either CPD or the IL method. For sectioning and observation, a wide range of the currents (38.6, 50, 240, 600 pA) and two FIB/SEM main detectors (SE, BSE) were applied to obtain precise images of the chromosome interiors. Detailed information regarding signal detectors, voltage, and other sectioning/observation conditions associated with each image are presented in Table 2.

Table 2. Dissection and observation conditions by FIB/SEM

Materials	Preparations	Machine	Dissection current probe *	Observation accelerating voltage**	Detectors	Corresponding figures
Barley	CPD	AURIGA 60	-	2.00	SESI (SE)	Fig. 31a
Barley	CPD	AURIGA 60	600	2.00	SESI (SE)	Fig. 31b, c, e
Barley	CPD	AURIGA 60	600	2.00	ESB (BSE)	Fig. 31b', c', e'
Barley	CPD	AURIGA 60	240	2.00	InLens (SE)	Fig. 31d
Barley	CPD	AURIGA 60	240	2.00	ESB (BSE)	Fig. 31d'
PA	CPD	SMI-3050	-	30.0	Lower (SE)	Fig. 32a, c
PA	CPD	JSM-7600F	38.6	5.0	LEI (SE)	Fig. 32b, d
PA	CPD	AURIGA 60	-	2.00	SESI (SE)	Fig. 32e
PA	CPD	AURIGA 60	120	2.00	InLens (SE)	Fig. 32f
Barley	IL	AURIGA 60	-	2.00	SESI (SE)	Fig. 33a
Barley	IL	AURIGA 60	240	2.00	SESI (SE)	Fig. 33b, d'
Barley	IL	AURIGA 60	240	2.00	InLens (SE)	Fig. 33c'
Barley	IL	AURIGA 60	240	2.00	ESB (BSE)	Fig. 33c'', d''
PA	IL	AURIGA 60	-	2.00	SESI (SE)	Fig. 34a
PA	IL	AURIGA 60	240	2.00	InLens (SE)	Fig. 34b, c
PA	IL	AURIGA 60	240	2.00	ESB (BSE)	Fig. 34b', c'
PA	IL	AURIGA 60	50	1.50	InLens (SE)	Fig. 34d
PA	IL	AURIGA 60	50	1.50	ESB (BSE)	Fig. 34d'

\* Unit is pico ampere (pA)

\*\* Unit is kilo volt (kV)

### 5.3.1 Chromosome prepared by CPD

Barley chromosomes prepared by the CPD method were dissected and observed by FIB/SEM as shown in Figure 35. The interior of barley chromosomes has been reported to be dominated by an extensive cavity network (Schroeder-Reiter *et al.*, 2009, 2012). The current results, however, showed two different types of chromosome interiors; some cross-sections and longitudinal-sections chromosome images revealed the existence of numerous cavities inside barley chromosomes treated with CPD (Figs. 35 B-C', E, E'), but others showed no cavities (Figs. 35D, D').



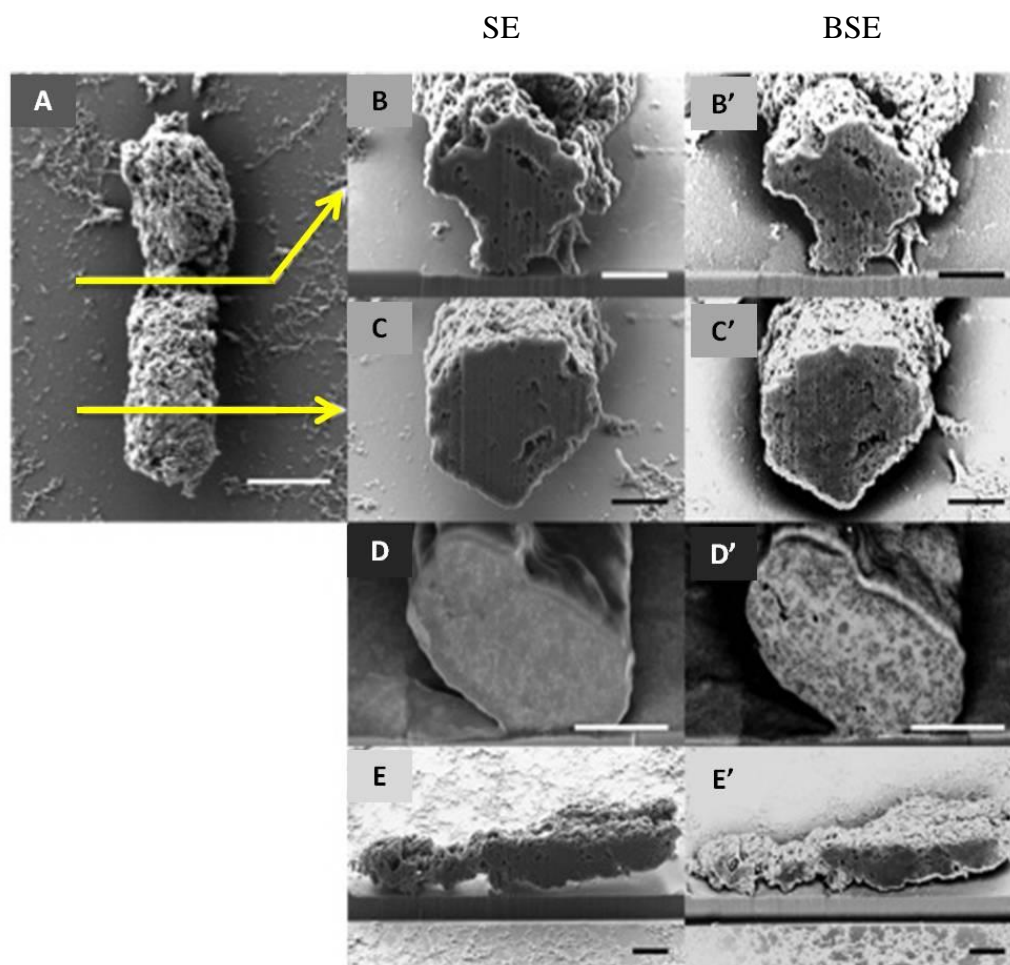


Figure 35. Whole image (A) and cross-sections (B-E') of barley chromosomes prepared by CPD. Chromosomes were dissected at the centromere and long arms as indicated by the white lines (A). Longitudinal cut chromosomes were also revealed (E and E'). Some cross-sections have cavities (B-C' and E, E') and the other cross-section from different chromosome do not (D, D'). Bars: 3  $\mu\text{m}$  (A, E, E'), 1  $\mu\text{m}$  (B-D'). Detectors: SE (B, C, D, E) and BSE (B', C', D', E').

The existence of cavities in some chromosomes prepared by CPD is consistent with previous reports (Schroeder-Reiter *et al.*, 2009, 2012). There were various sizes of cavities, ranging from 50 to 500 nm in diameter, with the majority being 50-100 nm (Figs. 35 B-C', E, E'). The cavities appeared to be distributed more or less randomly within the chromosome cross-sections and longitudinal-sections. They were visualized clearly by SE mode (Figs. 35B, C, E) as well as by BSE mode (Figs. 35B', C', E').

In some chromosomes, no cavities were visualized (Figs. 35D, D'), despite using the

same FIB/SEM sectioning conditions (current probe, voltage, and dwell time): the chromosome interior was revealed as a compact structure without any voids. In sample preparation for SEM, several steps are required before hydrated samples like most biological samples, including chromosomes. They must first be dehydrated and then dried before placing the specimen in the SEM sample chamber, because SEM is conducted under high vacuum conditions so that gas molecules do not interfere with the electron beam or the emitted secondary and backscattered electrons used for imaging. During sample preparation, some differences might occur which could not be exactly controlled. For example the critical point dryer could handle only four samples at once, and each experiment might involve minute differences that may cause different effects on the chromosome structure.

In this study, the first FIB/SEM images of human chromosomes are presented. As with the barley chromosomes, two types of chromosome interiors in terms of cavity existence were also found for human chromosomes prepared by CPD, as shown in Figure 36. Figures 36A, C, E depict low magnification images of human chromosomes. To investigate their interiors, chromosomes were dissected by FIB and then observed by SEM at high resolution (Figs. 36A', B', C'). As with barley chromosomes, the existence of cavities was also observed in only some of the human chromosomes. Further, some chromosomes did not show any cavity (Figs. 36B', C').

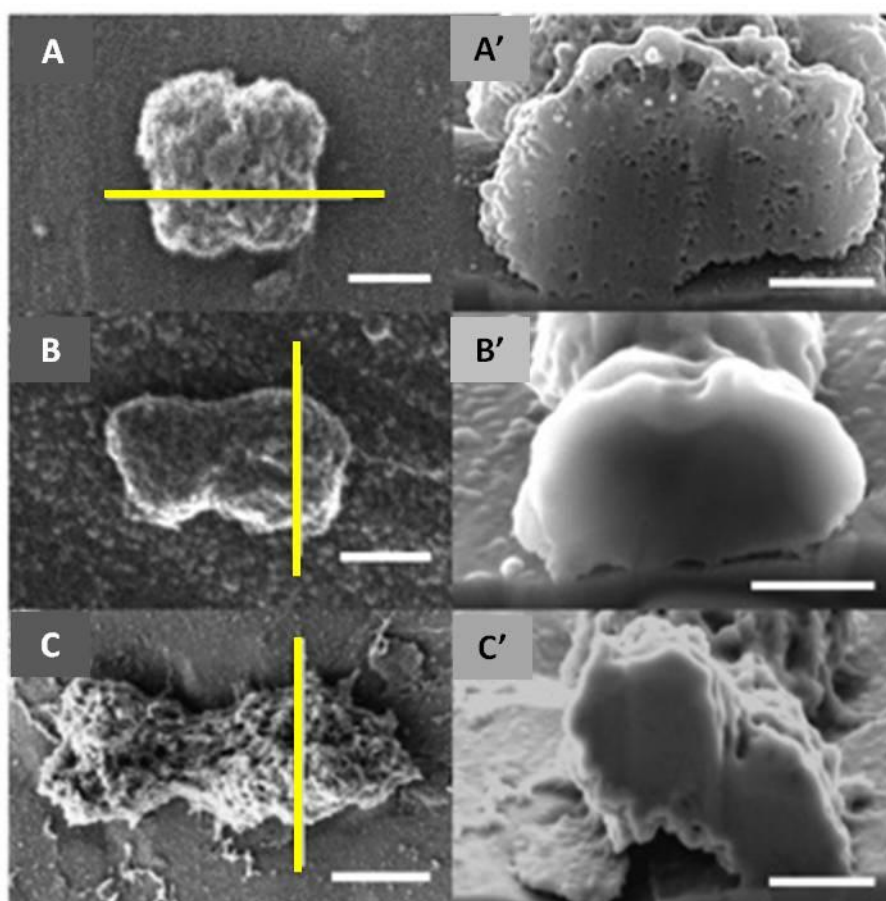


Figure 36. Whole images (A, B, C) and cross-sections (A', B', C') of PA chromosomes prepared by CPD. The yellow lines in A, B, and C indicate where the chromosomes were dissected. One cross-section has cavities A' and the others do not (B', C'). Bars: 1  $\mu$ m (A, B, C), 500 nm (A', B', C'). Detectors: combination of SE and BSE (A, B), SE (A', B', C, C').

Comparing barley and human chromosomes, barley chromosomes tended to show more cavities (Fig. 35) than human chromosomes (Fig. 36); most human chromosomes tended to show no cavities. When cavities were detected in human chromosomes, their number and sizes were smaller than those detected in barley chromosomes. The different cavity sizes between barley and human chromosomes might be explained by the different chromosome sizes. FIB sectioning conditions (current probe, voltage, dwell time) were different between barley and human chromosomes due to their size differences. The larger size of barley chromosomes often required stronger accelerating voltages and higher probe currents for them to be dissected.

The number, size, and pattern differences of cavities in each section may indicate the presence of various types of spaces within the chromosomes. These spaces may be enlarged/increased upon sample preparation, including the delicate steps of CPD. Further experiments will be required to test this hypothesis.

For many years, a variety of approaches have been combined to demonstrate the presence of scaffold proteins, and an alternating distribution of scaffold proteins along the chromosome arms has been reported (Maeshima and Laemmli, 2003; Ono *et al.*, 2004). With regards to the presence of cavities within chromosomes, chromosome interiors without cavities or with only small cavities may not conflict with this essential distribution of scaffold proteins at the axial regions of the chromatids.

### **5.3.2 Chromosome prepared with ionic liquid**

Barley and human chromosomes were also prepared by the IL method. This method enables us to skip EtOH dehydration, CPD, as well as metal coating. Instead of OsO<sub>4</sub> staining, we stained the chromosomes with Pt-blue. This rapid preparation method keeps the chromosomes closer to their natural conditions in terms of water content. FIB/SEM dissection/observation revealed that, in contrast to CPD-prepared chromosomes, there was no cavity in the chromosomes prepared with IL (Fig. 37C'-D''), using either SE or BSE detection.

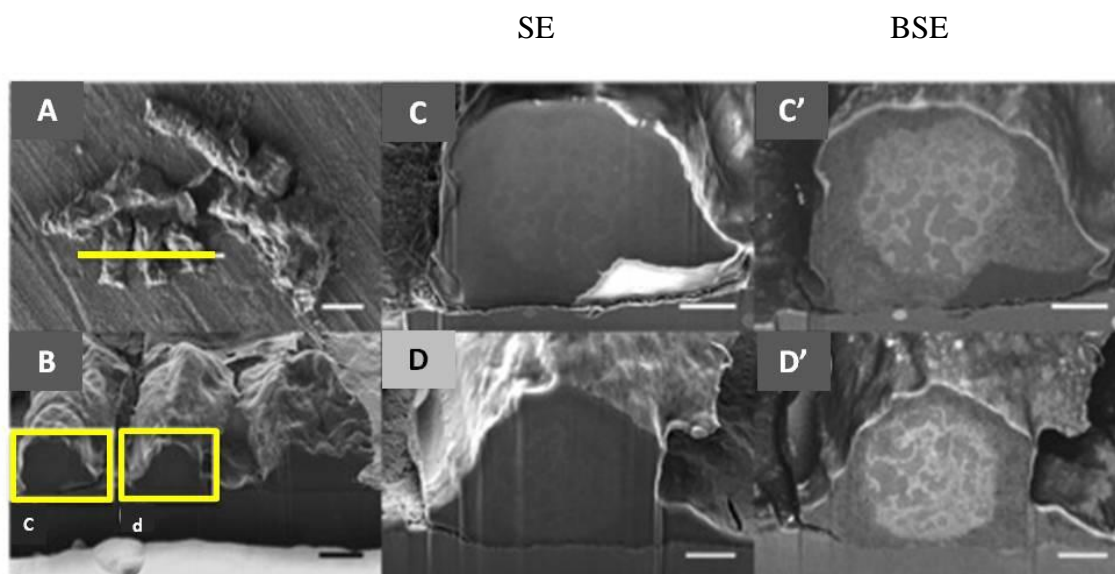


Figure 37. Whole image (A) and cross-sections (B-D') of barley chromosomes prepared with IL. No cavities are observed in the cross-sections. Bars: 10  $\mu\text{m}$  (A), 3  $\mu\text{m}$  (B), and 1  $\mu\text{m}$  (C-D'). Detectors: SE (C, D), and BSE (C', D').

Similar results were also obtained with human chromosomes prepared by the IL method, as presented in Figure 38. Simultaneous detection of SE and BSE signals showed that there were no cavities inside human chromosomes, as observed both in cross-section (Figs. 38B-C') as well as longitudinal-section images (Figs. 38D, D'). Accelerating voltages that controlled the speed of the  $\text{Ga}^+$  used for observation ranged from 1.5 to 2.0 kV. Different current conditions for chromosome sectioning, which controlled the number of  $\text{Ga}^+$  ions used for focus sectioning, were also applied. These different conditions all gave similar results, indicating that the lack of cavities is not caused by these particular parameters involved in sectioning/observation.

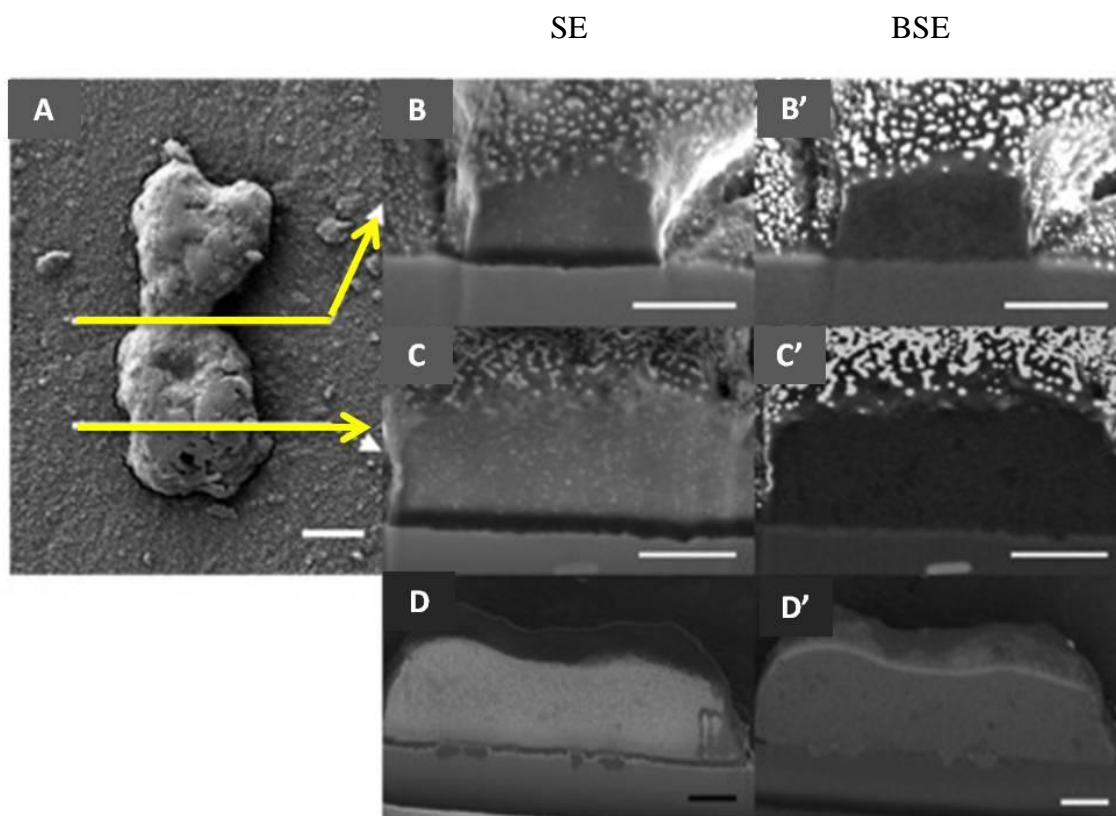


Figure 38. Whole image (A) and cross-sections (B-D') of human chromosomes prepared with IL. The white lines in (A) indicate where the chromosome was dissected. Cavities are not observed in any cross-sections, nor longitudinal-sections (D and D'). Bars: 1  $\mu\text{m}$  (a), 500 nm (B-D'). Detectors: SE (B, C, D), and BSE (B', C', D').

### 5.3.3 Nucleosome-like visualization within chromosome observed by FIB/SEM

Figure 39A depicts low magnification image of human chromosome before being sectioned by FIB. White arrows indicate the side of chromosome cross-sections which were imaged by SEM. After sectioning, the results showed the appearance of white dots within the chromosomes observed in only SE mode as revealed in Figures 39B, C, D, and E. These white dots are apparently distributed randomly within chromosome cross-sections and along the whole chromosome including chromosome arm (Fig. 39B, C) and centromere (Fig. 39D, E).



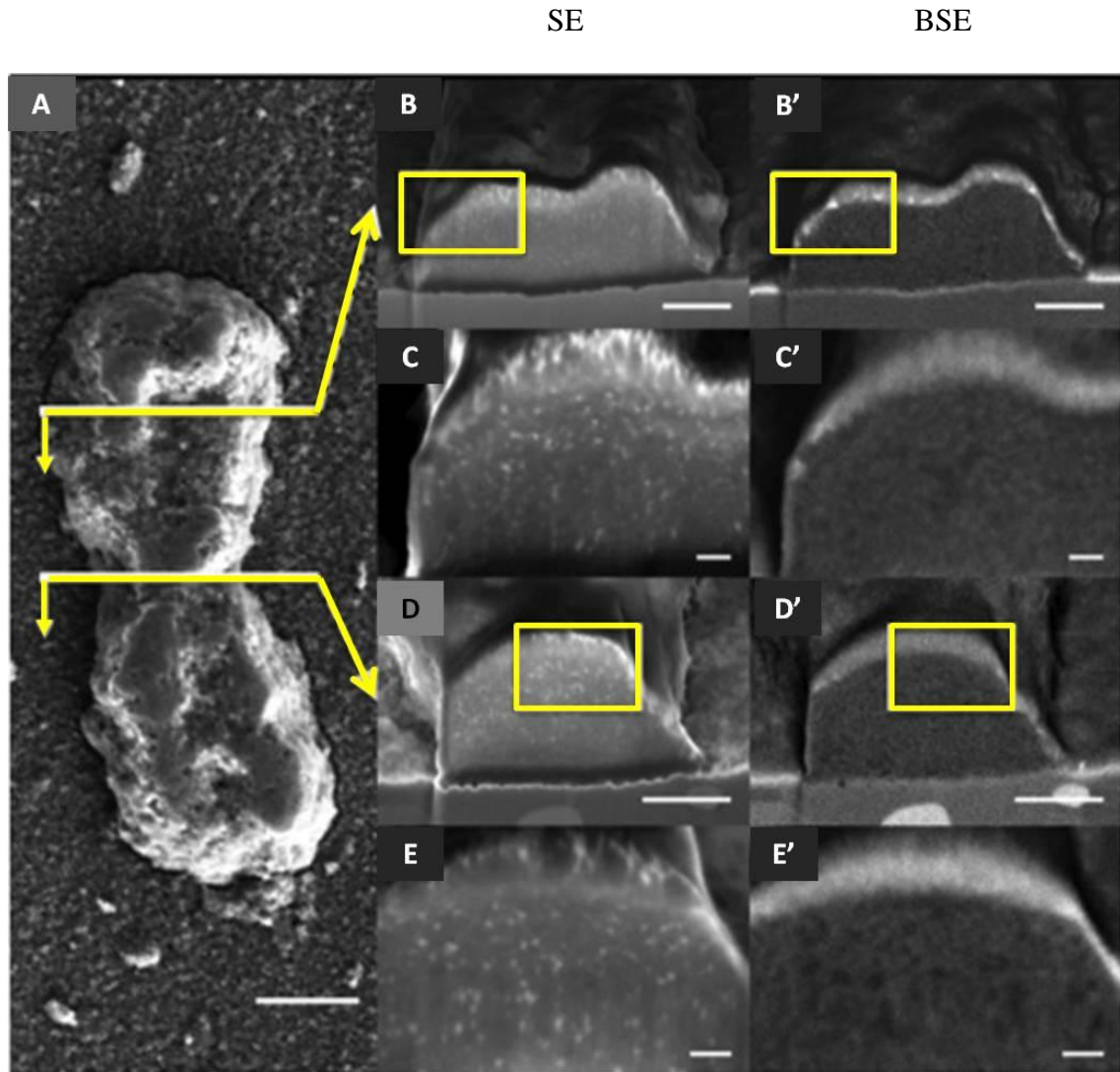


Figure 39. White dots visualization within chromosome. Chromosomes were dissected at chromosome arm and centromere as indicated by the white lines (A). Yellow arrows indicate the side of chromosome cross-sections which were imaged by SEM. Cross-sections imaged by SE mode show white dots distributed within chromosome interior (B, C, D, E), while those observed simultaneously by BSE mode do not (B', C', D', E'). Bars: 1  $\mu\text{m}$  (A), 500 nm (B, B', D, D'), 100 nm (C, C', E, E'). Detectors: SE (B, C, D), BSE (B', C', D').

To get the more detailed information about the relationship of white dots within chromosome cross-sections, sectioning was conducted continuously with the interval of 20 nm. The results indicated that among five slices with the interval of 20 nm, all slices showed different pattern of white dots positions. These results suggested that the white

dots are not the same structure from one slice to another and the size of each white dot is less than 20 nm.

Based on the data, the white dots were detected only by using SE mode, indicating the existence of certain structure on the cross-sections instead of a different atomic number within the chromosomes that may be caused by  $\text{Ga}^+$  beam damage or substrate sputtering. The fact that the white dots appeared in random pattern instead of completely covered the cross-section, supporting the idea that they were neither the sputtered aluminum nor the beam damage. However, the accumulation of electron charge in concave area could be another possibility to show bright signals. Further investigation should be required to prove it.

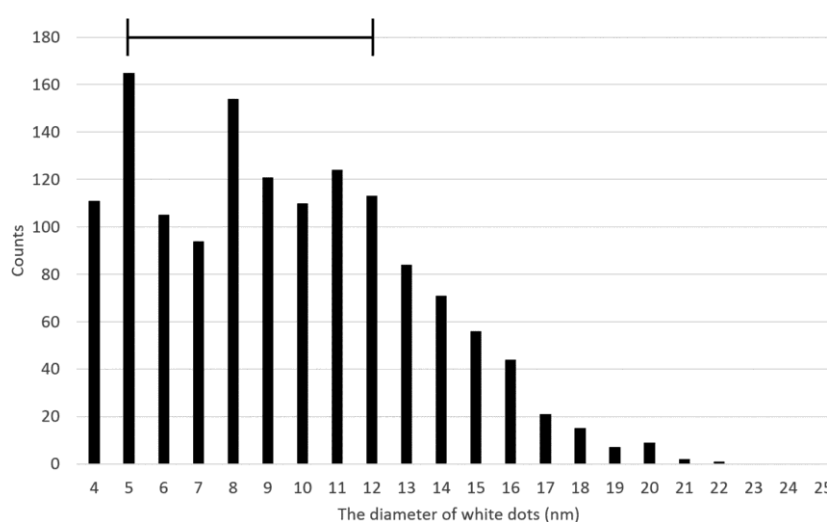


Figure 40. The graph of white dots diameters within chromosomes (5 cross-sections,  $n = 1407$ ). The high peaks distributed from 5 to 12 nm which represent close diameter of nucleosomes from the view of different angles (solid bar in the graph).

To gain deeper information of the white dots, the size of the white dots within chromosomes was further investigated by measuring the diameter of each dot and the results are presented in Figure 40. As shown in the figure, the average diameters of white dots ( $n = 1407$ ) are distributed in the range of 4 to 22 nm, with the high peaks distribution



at 5 to 12 nm. This range arose the idea that those white dots might be nucleosomes, although further proofs should obviously be necessary because there is also another possibility that those white dots might be chromatin-binding proteins.

Chromosome interior imaged by BSE mode did not show a strong contrast of the white dots as those detected by SE mode. This result might be affected by the low accelerating voltage (2 kV) as previously explained by Brodusch *et al.* (2014). The BSE micrograph at low kV provides the same contrast between different atoms. A strong different contrast was not achievable when the low voltage was used because of its small emission depth of the BSEs.

#### **5.3.4 Chromosome visualization by STEM tomography with IL method**

Chromosome images at 0° prepared with conventional and IL method were compared and the results were presented in Figure 41. Chromosome prepared with conventional method including dehydration and drying showed cloudy structure without any distinct particles shown in high magnification (Fig. 41A). In contrast, when the chromosome was prepared with the IL method without dehydration and drying, white dots were detected composing the chromosome structure. These white dots were distributed throughout the chromosome body and have the diameter of 10-20 nm (Fig. 41B).

By considering the preparation method (avoiding dehydration and drying) and the diameter of white dots particles, similar idea with the FIB/SEM results arose, suggesting that those white dots might represent nucleosomes. And those structures could be attached to each other and shrank by the harsh steps of dehydration and drying. Further investigation would be necessary to prove this hypothesis.

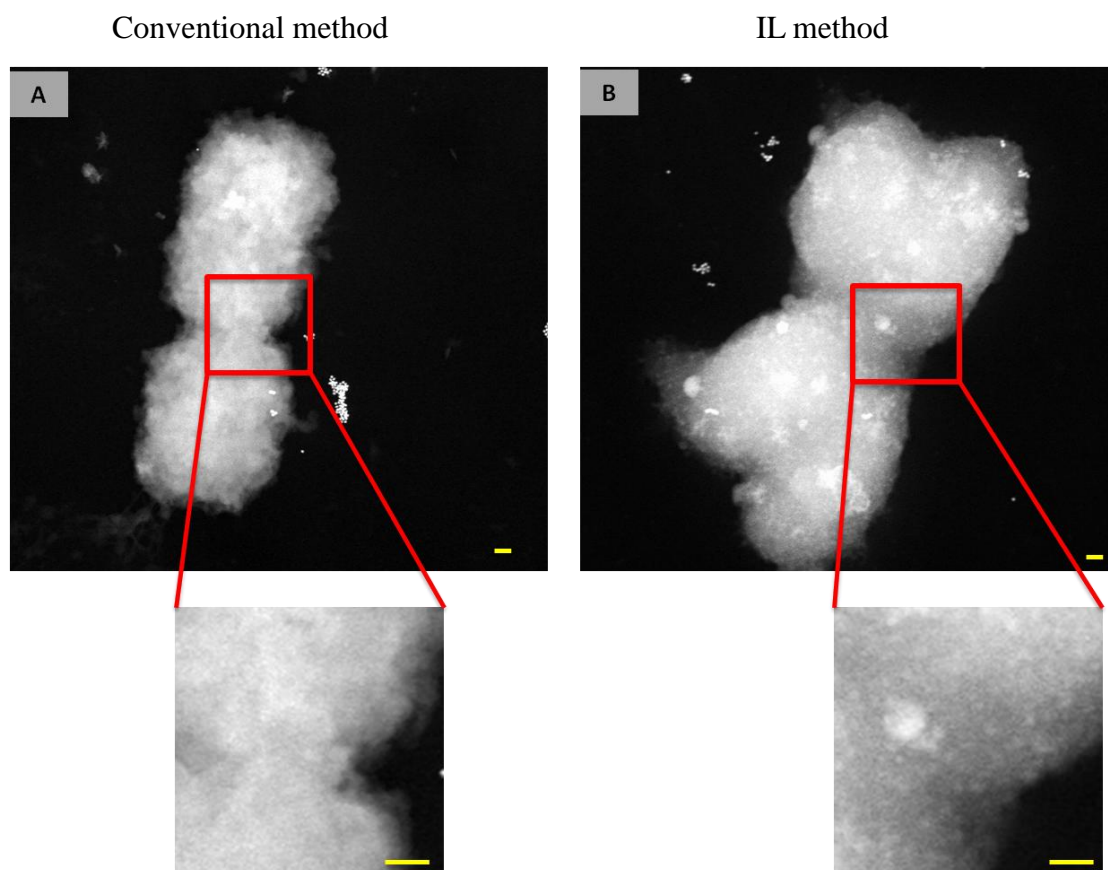


Figure 41. Chromosomes at  $0^\circ$  showed different structure according to different preparation methods. White dots were detected only when the chromosome was treated with IL. Bars: 100 nm.

#### 5.4 Discussion

In this study, chromosome interior was investigated by FIB/SEM using plant (barley) and human chromosomes prepared by the conventional (CPD) and IL method. As a result, two types of chromosomes, with and without cavities, were visualized, both for barley and human chromosomes prepared by CPD. However, chromosome interiors were revealed only as a solid structure, lacking cavities, when prepared by the IL method. The results suggest that the existence and sizes of cavities depend on the preparation procedures.

Previous results show that the IL method could successfully be applied to the visualization of chromosome higher-order structure by SEM without dehydration and

metal coating. Sample preparation for SEM can be completed within minutes and leads to no serious changes in sample morphology.

By considering the properties of ionic liquid, the varied results of chromosome interior prepared with CPD, the similar results in different sectioning/observing parameters, and the established report of the alternative distribution of scaffold proteins within chromosome arms, FIB/SEM investigation of chromosome interior suggests the more flexible structure of chromosome interior with regards to the presence/absence of cavity. In addition, the size of cavity might be enlarged by dehydration/drying process.

Nucleosome, a primary structure of DNA compaction that wrapped around the core histone octamer, has excessively been investigated by X-ray crystallography (Wilkin and Zubay 1959, Richards and Pardon 1970) and its structure within the digested chromatin by micrococcal nuclease has been studied by electron microscopy (Finch *et al.* 1975, Finch and Klug 1976), showing the basic structure of chromosome condensation arranged in beads-on-string pattern with the diameter of 11 nm. However, information concerning this structural observation within the intact metaphase chromosome in high resolution remains enigmatic. Based on the results, the white dots were visualized within the chromosome. The distribution, shape, and size of the white dots indicating that those white dots might be the nucleosomes.

## **5.5 Summary**

In this study, an insight with regard to different types of chromosome interior has been gained: with and without cavities. The feasibility and the efficacy of the IL method in conjunction with FIB/SEM for chromosome analysis were also examined. Based on the results obtained, the combination of the IL method with the advantages of FIB/SEM in slicing chromosomes provides a new method for investigating the interior of

chromosomes in the condition closer to native one. The application of the IL method should enable new developments in sample observation methods. The benefits of FIB/SEM for chromosome sectioning in conjunction with the IL method have been presented to gain an insight into chromosome interior in a rapid, easy, and practical manner. This combination would also be promising for other biological sample investigation.

Herein, the first finding of white dots within the chromosomes as observed by FIB/SEM prepared by the IL method and stained with Pt-blue tomography is reported. The different pattern of white dots in each chromosome slices observed in SE mode and the average diameter of the white dots suggested a unique structure within chromosome leading to the first visualization of nucleosome-like structure.

## **Chapter 6**

### **General conclusion**

In this study, the effect of  $\text{Ca}^{2+}$  and  $\text{Mg}^{2+}$  on the chromosome structure was evaluated. The results demonstrated the changes of chromosome structure dependent on the  $\text{Ca}^{2+}$  and/or  $\text{Mg}^{2+}$  concentration, suggesting the importance of these divalent cations for the structural maintenance of the chromosome.

In addition, the application of new visualization methods including HIM, IL method, and FIB/SEM was simultaneously performed. These newly developed methods were successfully proven to be beneficial for chromosome study with regards to the rapid and closer to the native state preparation steps. Furthermore, the use of FIB/SEM gave another insight into the chromosome interior structure especially when the samples were prepared using the IL method.

In chapter 2, the changes of chromosome structure in different concentration of  $\text{Ca}^{2+}$  and  $\text{Mg}^{2+}$  were presented. After  $\text{Ca}^{2+}$  depletion by using BAPTA (AM), chromatin diameter was decreased. Interestingly, after re-addition of  $\text{Ca}^{2+}$ , chromosome structure returned to its original form. Similar results were also obtained when two different  $\text{Mg}^{2+}$  concentrations was applied. Chromosome shown as a compact structure with granular chromatin structure when it was treated with buffer containing 5 mM  $\text{Mg}^{2+}$ . However, when the buffer containing 0 mM  $\text{Mg}^{2+}$  was used, chromosome showed the more decondensed structure with smaller chromatin fibers. Reversibility of these changes was shown after re-addition of 5 mM  $\text{Mg}^{2+}$ . When EDTA which can chelate both  $\text{Ca}^{2+}$  and  $\text{Mg}^{2+}$  was applied, chromosome resulted in the similar structural deformation with those treated with 0 mM  $\text{Mg}^{2+}$  and  $\text{Ca}^{2+}$  depletion. The effect of  $\text{Mg}^{2+}$  was also confirmed by using STEM tomography which enables us to see the 3D structure of the sample by tilting the sample stage. The data obtained showed that chromosome treated with 0 mM  $\text{Mg}^{2+}$  has a dispersed and fibrous structure compared with those treated with 5 mM  $\text{Mg}^{2+}$ . Altogether, these results suggest that divalent cations play an important role in the

maintenance of chromosome structure. In addition, the chromatin structure undergoes reversible changes.

The advantages of technology development have also been assessed in this study to gain the deeper understanding on the chromosome structure by solving the limitation of the conventional method. One major problem in the conventional method is that the possibility of artifact induced by metal coating as reported previously (Pretorius, 2010). The presence of coating material may hide the actual surface structure of the chromosome. Thus, in this study new visualization methods were developed to avoid the metal coating for chromosome visualization.

In Chapter 3, the results of HIM observation were presented. According to the data obtained, for the first time chromosome could be clearly visualized by using HIM even without metal coating. Uncoated chromosome was revealed in high resolution and contrast. The 11 nm fibers could clearly be observed. In addition, the different structure of chromosome in different concentration of  $\text{Mg}^{2+}$  was also described. As compared to SEM, HIM images gave a higher resolution and detailed surface structure. The diameter of chromatin shown in HIM image was also smaller than that of SEM image, suggesting the thickness of coating material ( $\text{OsO}_4$ ) on the SEM image. These results indicate that the charging controller in HIM system is efficient to avoid charging up phenomenon in nonconductive samples. Thus it proves the advantages of HIM that can also be applied for other biological samples to gain the more detailed structure.

Furthermore, not only metal coating, other preparation steps for SEM observation including dehydration and drying have also been reported to cause shrinkage and artifact (Schatten, 2011). In this study, the IL method was developed to avoid the defect of dehydration and drying method as well as to avoid metal coating. In addition, since the samples were not dried because of the negligible volatility of IL, it is said that the IL

method can maintain the condition of the biological samples in the condition closer to their native one. Based on the results obtained, chromosome could be visualized by using SEM for the first time even without dehydration, drying, and metal coating. As compared to the conventional sample preparation methods, the IL is a quick and efficient method to study chromosome higher-order structure by SEM. Furthermore, the optimum conditions for the IL method were investigated in this study. The use of low concentration (0.5-1%) BMI-BF<sub>4</sub> and the combination of IL with Pt-blue can enhance the contrast and resolution of the IL-treated chromosome image observed by SEM. The exploration of IL method to gain the higher resolution chromosome images was also performed by combining the IL method with HIM. This combination yields the clearer chromosome images with high resolution and stronger contrast compared with those taken by SEM.

Finally, to get the deeper and comprehensive information of chromosome structure, not only the surface investigation by HIM and IL method, but also the chromosome interior was assessed in this study by using FIB/SEM. The results showed two types of interior, with and without cavities, when chromosome was prepared with the conventional method. The combination of the IL method and FIB/SEM were effective to give another insight of the chromosome interior, especially with regards to the absence of the cavities within chromosome. By using the IL method, the chromosome interior was shown as a solid structure without any cavity. The less number or even the absence of the cavity will not interfere with the nice arrangement of scaffold proteins within the chromosome previously reported (Ono, 2004). Furthermore, in this study, chromosome interior investigation by FIB/SEM in conjunction with IL method, as well as the confirmation by STEM tomography in conjunction with IL, demonstrated the white dots visualization within the chromosomes. The number, size, and pattern of those white dots leading to a hypothesis of first visualization of nucleosome structure within chromosome, although



further evidence would be required.

All of these data suggesting that the IL method developed in this study is advantageous for chromosome research. In conclusion, the limitations of sample preparation for chromosome observation by SEM have been remarkably overcome by developing the IL method. This new method has successfully been demonstrated to be applicable for other systems including HIM in providing high-resolution chromosome images, FIB/SEM in presenting chromosome interior information, and STEM tomography in imaging 3D chromosome. These methods enable us to observe chromosome surface and interior in high resolution, rapid, and closer to their native condition by avoiding dehydration, drying, and metal coating. The results achieved in this study would contribute not only to further chromosome research but also to the other biological samples visualization.

## References

- Abramoff MD, Magalhaes PJ, and Ram SJ** (2004). Image processing with ImageJ. *Biophoton Intern* 11: 36-42.
- Adolph KW, Kreisman LR, and Kuehn RL** (1986). Assembly of chromatin fibers into metaphase chromosomes analyzed by transmission electron microscopy and scanning electron microscopy. *Biophys J* 49: 221-231.
- Bell DC** (2009). Contrast mechanisms and image formation in helium ion microscopy. *Microsc Microanal* 15: 147-153.
- Bian Q, and Belmont AS** (2012). Revisiting higher-order and large-scale chromatin organization. *Curr Opin Cell Biol* 24: 359-366.
- Boyde A, and Boyde S** (1980). Further studies of specimen volume changes during processing for SEM: including some plant tissue. *Scan Electron Microsc* 132: 117-124.
- Boyde A, and Maconnachie E** (1979). Volume changes during preparation of mouse embryonic tissue for SEM. *Scanning* 2: 149-163. In: Schatten H (2011). Low voltage high-resolution SEM (LVHRSEM) for biological structural and molecular analysis. *Micron* 42: 175-185.
- Boyde A, and Maconnachie E** (1981). Morphological correlations with dimensional change during SEM specimen preparation. *Scan Electron Microsc* 4: 27-34.
- Brodusch N, Waters K, Demers H, and Gauvin R** (2014). Ionic liquid-based observation technique for nonconductive materials in the scanning electron microscope: Application to the characterization of a rare earth one. *Microsc Res Tech* 77: 225-235.
- Bushby AJ, Ping KM, Young RD, Pinali C, Knupp C, and Quantock AJ** (2011).

Imaging three dimensional tissue architectures by focused ion beam scanning electron microscopy. *Nat Protocol* 6: 856-858.

**Caravaca JM, Caño S, Gállego I, and Daban J** (2005). Structural elements of bulk chromatin within metaphase chromosomes. *Chromosome Res* 13: 725-743.

**Cole A** (1967). Chromosome structure. In: *Theoretical and Experimental Biophysics: A series of Advances*. Cole, A. (Ed.), Vol. 1: pp. 305-375. New York: Marcel Dekker.

**Drobne D, Milani M, Lešer V, and Tatti F** (2007). Damage induced by FIB milling samples is controllable. *Microsc Res Tech* 70: 895-903.

**Dwiranti A, Hamano T, Takata H, Nagano S, Guo H, Ohnishi K, Wako T, Uchiyama S, and Fukui, K** (2014). The Effect of Magnesium Ions on Chromosome Structure as Observed by Helium Ion Microscopy. *Microsc Microanal* 20: 184-188.

**Dwiranti A, Lin L, Mochizuki E, Kuwabata S, Takaoka A, Uchiyama S, and Fukui K** (2012). Chromosome observation by scanning electron microscopy using ionic liquid. *Microsc Res Tech* 75: 1113-1118.

**Earle MJ, and Seddon KR** (2000). Ionic liquids: Green solvents for the future. *Pure Appl Chem* 72: 1391-1398.

**Eltsov M, Maclellan KM, Maeshima K, Frangakis AS, and Dubochet J** (2008). Analysis of cryo-electron microscopy images does not support the existence of 30-nm chromatin fibers in mitotic chromosomes in situ. *Proc Natl Acad Sci* 105: 9732-9737.

**Engelhardt M** (2004). Condensation of chromatin in situ by cation-dependent charge shielding and aggregation. *Biochem Biophys Res Commun* 324:1210-1214.

**Finch JT, and Klug A** (1976). Solenoidal model for superstructure in chromatin. *Proc Natl Acad Sci* 73: 1897-1901.

**Finch JT, Noll M, and Kornberg RD** (1975). Electron microscopy of defined lengths of

chromatin. *Proc Natl Acad Sci* 72, 3320-3322.

**Forsyth SA, Pringle JM, and MacFarlane DR** (2004). Ionic liquids - an overview. *Aust J Chem* 57: 113-119.

**Frank J** (1992) *Electron Tomography: three-dimensional imaging with the transmission electron microscope*. pp. 1-399, New York: Plenum Press.

**Friedmann A, Hoess A, Cismak A, and Heilmann A** (2011). Investigation of cell-substrate interaction by focused ion beam preparation and scanning electron microscopy. *Acta Biomaterial* 7: 2499-2507.

**Fukui K** (2009). Structural analyses of chromosomes and their constituent proteins. *Cytogenet Genome Res* 124: 3-4.

**Fukui K, and Kakeda K** (1991). Quantitative karyotyping of barley chromosomes by image analysis methods. *Genome* 33: 450-458.

**Fukui K, and Uchiyama S** (2007). Chromosome protein framework from proteome analysis of isolated human metaphase chromosomes. *Chem Rec* 7: 230-237.

**Grigoryev SA, and Woodcock CL** (2012). Chromatin organization - the 30 nm fiber. *Exp Cell Res* 318: 1448-1455.

**Hagiwara R, and Ito Y** (2000). Room temperature ionic liquids of alkylimidazolium cations and fluoroanions. *J Fluorine Chem* 105: 221-227.

**Hayashihara K, Uchiyama S, Kobayashi S, Yanagisawa M, Matsunaga S, and Fukui K** (2008). Isolation method for human metaphase chromosome. *Protoc Exchange*. DOI:10.1038/nprot.2008.166.

**Inaga S, Katsumoto T, Tanaka K, Kameie T, Nakane H, and Naguro T** (2007). Platinum blue as an alternative to uranyl acetate for staining in transmission electron microscopy. *Arch Histol Cytol* 70: 43-49.

**Ishigaki Y, Nakamura Y, Takehara T, Nemoto N, Kurihara T, Koga H, Nakagawa H,**

- Takegami T, Tomosugi N, Miyazawa S, and Kuwabata S** (2011). Ionic liquid enables simple and rapid sample preparation of human culturing cells for scanning electron microscope analysis. *Microsc Res Techniq* 74: 415-420.
- Kuwabata S, Kongkanand A, Oyamatsu D, and Torimoto T** (2006). Observation of ionic liquid by scanning electron microscope. *Chem Lett* 35: 600-601.
- Kuwabata S, Tsuda T, and Torimoto T** (2010). Room-temperature ionic liquid: A new medium for material production and analyses under vacuum conditions. *J Phys Chem Lett* 1: 3177-3188.
- Luger K, Mader AW, Richmond RK, Sargent DF, and Richmond TJ** (1997). Crystal structure of the nucleosome core particle at 2.8 Å resolution. *Nature* 389: 251-260.
- Maeshima K, and Laemmli UK** (2003). A two-step scaffolding model for mitotic chromosome assembly. *Dev Cell* 4: 467-480.
- Nishino Y, Eltsov M, Joti Y, Ito K, Takata H, Takahashi Y, Hihara S, Frangakis AS, Imamoto N, Ishikawa T, and Maeshima K** (2012). Human mitotic chromosomes consist predominantly of irregularly folded nucleosome fibres without a 30-nm chromatin structure. *EMBO* 31: 1644-1653.
- Nishiyama H, Suga M, Ogura T, Maruyama Y, Koizumi M, Mio K, Kitamura S, and Sato C** (2010). Atmospheric scanning electron microscope observes cells and tissues in open medium through silicon nitride film. *J Struct Biol* 172: 191-202.
- Okazaki K, Kiyama T, Hirahara K, Tanaka N, Kuwabata S, and Torimoto T** (2008). Single-step synthesis of gold-silver alloy nanoparticles in ionic liquids by a sputter deposition method. *Chem Commun* 691-693.
- Ono T, Fang Y, Spector DL, and Hirano T** (2004). Spatial and temporal regulation of condensins I and II in mitotic chromosome assembly in human cells. *Mol Biol Cell* 15: 3296-3308.

- Palacio M, and Bhushan B** (2010). A review of ionic liquids for green molecular lubrication in nanotechnology. *Tribol Lett* 40: 247-268.
- Pretorius E** (2011). Traditional coating methods in scanning electron microscopy compared to uncoated charge compensator technology: looking at human blood fibrin networks with the zeiss ultra plus FEG-SEM. *Microsc Res Techniq* 74: 343-346.
- Richard BM, and Pardon JF** (1970). The molecular structure of nucleohistone (DNH). *Exp Cell Res* 62, 184-196.
- Ris H** (1985). The cytoplasmic filament system in critical point dried whole mounts and plastic-embedded sections. *J Cell Biol* 100: 1474-1487.
- Schatten H** (2011). Low voltage high-resolution SEM (LVHRSEM) for biological structural and molecular analysis. *Micron* 42: 175–185.
- Schroeder-Reiter E, Sanei M, Houben A, and Wanner G** (2012). Current SEM techniques for de- and reconstruction of centromere to determine 3D CENH3 distribution in barley mitotic chromosomes. *J Microsc* 246: 96-106.
- Schroeder-Reiter E, Pérez-Willard F, Zeile U, and Wanner G** (2009). Focused ion beam (FIB) combined with high resolution scanning electron microscopy: a promising tool for 3D analysis of chromosome architecture. *J Struct Biol* 165: 97-106.
- Torimoto T, Okazaki K, Kiyama T, Hirahara K, Tanaka N, and Kuwabata S** (2006). Sputter deposition onto ionic liquids: simple and clean synthesis of highly dispersed ultrafine metal nanoparticles. *Appl Phys Lett* 89: 243117. DOI: 10.1063/1.2404975.
- Ushiki T, Shigeno M, and Hoshi O** (2008). Methods for imaging human metaphase chromosomes in liquid conditions by atomic force microscopy. *Nanotech* 19: 384022. DOI:10.1088/0957-4484/19/38/384022.
- Uchiyama S, Doi T, and Fukui K** (2008). Isolation of human and plant chromosomes as nanomaterials. In: *chromosome nanoscience and technology*. Fukui K and Ushiki T

(ed.), pp 155-166. UK: CRC Press,

**Uchiyama S, Kobayashi S, Takata H, Ishihara T, Hori N, Higashi T, Hayashihara K,**

**Sone T, Higo D, Nirasawa T, Takao T, Matsunaga S, and Fukui K** (2005).

Proteome analysis of human metaphase chromosomes. J Biol Chem 280: 16994-17004.

**Uchiyama S, Kobayashi S, Takata H, Ishihara T, Sone T, Matsunaga S, and Fukui K**

(2004). Protein composition of human metaphase chromosomes analyzed by two-dimensional electrophoreses. Cytogenet Genome Res 107: 49-54.

**Wanner G, and Formanek H** (1995). Imaging of DNA in human and plant

chromosomes by high-resolution scanning electron microscopy. Chrom Res 3: 368-374.

**Ward BW, Notte JA, and Economou NP** (2006). Helium Ion Microscope: A new tool

for nanoscale microscopy and metrology. J Vac Sci Technol 24: 2871-2874.

**Welton T** (1999). Room-temperature ionic liquids: solvents for synthesis and catalysis.

Chem Rev 99: 2071-2084.

**Widom J, and Klug A** (1985). Structure of the 300A chromatin filament: Xray

diffraction from oriented samples. Cell 43: 207-213.

**Wilkes JS, and Zaworotko MJ** (1992). Air and water stable

1-ethyl-3-methylimidazolium based ionic liquids. J Chem Soc, Chem Commun 13: 965-967.

**Wilkin MHF, and Zubay G** (1959). X-ray diffraction studies of the molecular structure

of nucleohistone and chromosomes. J Mol Biol 1: 179-185.

**Woodcock CL and Ghosh RP** (2010). Chromatin higher-order structure and dynamics.

Cold Spring Harb Perspect Biol 2: a000596.

**Wurster D, and Benirschke K** (1970). Indian mutjac, *Muntiacus muntjak*: A deer with a

low diploid chromosome number. *Science* 168: 1364-1366.

**Yoshida K, Nozaki T, Hirayama T, and Tanaka** (2007). In situ high-resolution transmission electron microscopy of photocatalytic reactions by excited electrons in ionic liquid. *Journal of Electron Microscopy* 56: 177-180.



## List of publications

1. Dwiranti A, lin L, Mochisuki E, Kuwabata S, Takaoka A, Uchiyama S, Fukui, K. 2012. Chromosome Observation by Scanning Electron Microscopy using Ionic Liquid. *Microscopy Research and Method* 75: 1113-1118 doi: 10.1002/jemt.22038.
2. Dwiranti A, Hamano T, Takata H, Nagano S, Guo H, Ohnishi K, Wako T, Uchiyama S, Fukui, K. 2014. The Effect of Magnesium Ions on Chromosome Structure as Observed by Helium Ion Microscopy. *Microscopy and Microanalysis* 20: 184-188. doi:10.1017/S1431927613013792.
3. Hamano T, Dwiranti A, Kaneyoshi K, Fukuda S, Kometani R, Nakao M, Takata H, Uchiyama S, Ohmido N, Fukui K. Chromosome Interior Observation by Focused Ion Beam/Scanning Electron Microscopy (FIB/SEM) using Ionic Liquid Method. *Microscopy and Microanalysis* (In Press).

## Acknowledgements

I would like to express my gratitude to all those who gave me the possibility to complete this thesis. First and foremost, I wish to express my deepest and sincere gratitude to my supervisor, Professor Kiichi Fukui, for kindly giving me permission to commence research and complete this thesis in the Laboratory of Dynamic Cell Biology, Department of Biotechnology, Graduate School of Engineering, Osaka University. His guidance, advice, wisdom, and times have been of great value for me.

I am deeply indebted to Associate Professor Susumu Uchiyama, Associate Professor Suguru Tsuchimoto, Assistant Professor Hideaki Takata, Assistant Professor Hiroe Sakai, and Assistant Professor Naoki Wada for their valuable supervision, guidance, and excellent encouragement to me throughout this study.

I am also grateful to Professor Shinegori Kanaya, Professor Hajime Watanabe, and all Professors in Department of Biotechnology, Graduate School of Engineering, Osaka University for their valuable suggestions on my study.

I would like to express my cordial thanks to Professor Susumu Kuwabata and Mrs. Eiko Mochisuki, at Department of Applied Chemistry, Osaka University, Professor Toshiaki Suhara and Professor Akio Takaoka at Research center for Ultrahigh Resolution Electron Microscopy, Osaka University, for generously providing reagents for electron microscopic experiments and permission for using the facilities. I have furthermore to convey my appreciation to Dr. Tomoki Nishida, Dr. Yoshinori Muranaka, Dr. Ryusuke Kuwahara, and Mr. Toshiaki Hasegawa at Research center for Ultrahigh Resolution Electron Microscopy, Osaka University who always provided me valuable help, meticulous guidance, and great support in assisting me in my research which are indispensable to the completion of this study.

I owe special thanks to Dr. Keiko Ohnishi, Dr. Guo, and Mrs. Shoko Nagano at National Institute for Material Science, Tsukuba, Dr. Toshiaki Wako at National Institute of Agrobiological Sciences, Tsukuba, Dr. Shinichi Ogawa and Dr. Tomohiko Iijima at National Institute of Advanced Industrial Science and Technology, Tsukuba. Especially I am obliged to, Assist. Prof. Sumire Inaga at Medical Department, Tottori University. Assist. Prof. Megumi Iwano at Osaka University, Dr. Hitomi Ichikawa at Nara Advanced Institute of Science and Technology, Nara, and Prof. Nobuko Ohmido at Medical Department, Kobe University for invaluable suggestions and important knowledge. I am also thankful to Dr. Takuma Kanesaki, Dr. Peter Gnauck, and Dr. Henry Chai at Zeiss Laboratory for their great support. I am honored to express my gratitude to the Japanese government (Monbukagakusho) for financial support to do research at Department of Biotechnology, Graduate School of Engineering, Osaka University.

My appreciation is also extended to all members of Laboratory of Dynamic Cell Biology (Fukui Lab.) for their support and the good memories. I wish to thank Mr. Tomoyuki Doi, Ms. Junko Tanaka, Ms. Mari Iguchi for their administrative supports. Special thanks are also extended to the members of Chromosome Comprehensive Group, Ms. Rawin Poonperm, Ms. Rinyaporn Phengchat, Mr. Tosho Kondo, Mr. Kohei Kaneyoshi, Mr. Shota Fukuda, Ms. Gina Ratnasari, Mrs. Leung Wing Yan, Mr. Yusuke Nakao, and Ms. Marliza Madung who are always supportive. My special gratitude goes to Dr. Linyen Lin, Mrs. Ilma Equilibrina and Mr. Tohru Hamano for their kind help, and to all students in Fukui Lab. Finally, I would like to express my deepest gratitude to my parents, my husband Nadhif Rahmawan, my beloved daughter Akiranaya Dhifta Rahmawan, and all my dearest family and friends who have never failed to give their whole supports, guidance, prayers, and loves.